OFDM Transmission for Doubly Dispersive Underwater Acoustic Channels

by

Ali M. Bassam

Submitted in partial fulfillment of the
requirements for the degree of Master of Applied Science

at

Dalhousie University
Halifax, Nova Scotia
March 2015

Dedication

To my beloved mother and father

Table of Contents

List of Figures

Abstract

In this thesis, an OFDM simulator is designed based on the theory presented, and tested with a real underwater acoustic (UWA) channel. The UWA channel is analyzed and a simplified model is presented that holds under achievable conditions. The SOS model is developed for the UWA channel, and uses the stretched exponential function to model the Doppler power spectrum. The result is an SOS simulator which is then added to the OFDM simulator. The OFDM simulators are shown to have a very good performance under real, quasi-stationary UWA channels.

OFDM theory is presented and then applied to the UWA channel to combat frequency-selectivity. OFDM transmission on UWA channels is analyzed in great detail, with special emphasis on how the Doppler effect distorts the signal. A complete model which shows the channel effects on the received signal is developed. This is followed by ICI parametrization and two methods of Doppler compensation.

List of Abbreviations and Symbols Used

N	The number of subcarriers in an OFDM symbol, also the number of samples of the corresponding discrete-time sequence
f_k	The OFDM symbol's kth subcarrier frequency
Δf	The OFDM symbol's subcarrier spacing or subchannel bandwidth (or symbol rate under ideal conditions)
T	The OFDM symbol duration
T_s	Single-carrier symbol duration, also the sampling period of the OFDM symbol
$x(t)$	Transmitted baseband signal
$X[k]$	The DFT of $x(t)$, also the kth constellation point
$g(t)$	The transmit interpolation filter
$s(t)$	Transmitted passband signal
f_c	Carrier frequency
$y(t)$	Received baseband signal
$n(t)$	Passband noise signal
$q(t)$	The matched filter
$z(t)$	The filtered baseband noise signal
N_{cp}	Number of symbols, or length, of the cyclic prefic
$r(t)$	Received passband signal
$h(t,\tau)$	Bandpass impulse response of the channel
$h_p(t,\tau)$	The pth path's bandpass attenuation factor or impulse response of the underwater acoustic channel

$h_p(t)$	The pth path's bandpass attenuation factor simplified by the narrowband assumption
$\tau_p(t)$	The pth path's time-varying propagation delay
$\tilde{n}(t)$	Baseband noise signal
$\theta_p(t)$	Phase offset of the pth path at the baseband, $:= -2\pi f_c \tau_p(t)$
$c(t, \tau)$	Lowpass impulse response of the channel
$c_p(t, \tau)$	The pth path's lowpass attenuation factor or impulse response of the underwater acoustic channel
$c_p(t)$	The pth path's lowpass attenuation factor simplified by the narrowband assumption
$R_c(t_1, t_2, \tau_1, \tau_2)$	The autocorrelation function of $c(t, \tau)$
$R_c(\tau)$	The channel's multipath intensity profile or delay power spectrum
T_m	multipath (or delay) dispersion or spread
$R_C(t_1, t_2, f_1, f_2)$	The autocorrelation function of $C(t, f)$, also the 1-dimensional Fourier transform of $R_c(t_1, t_2, \tau_1, \tau_2)$
B_{coh}	The channel's coherence bandwidth, $:= 1/T_m$
ν	Doppler frequency
$S_C(\nu)$	The channel's Doppler power spectrum
B_d	The channel's Doppler spread
T_{coh}	The channel's coherence time, $:= 1/B_d$
l	Transmission distance
$A(l, f)$	Path loss
$a(f)$	Absorption coefficient
κ	Path loss exponent, which models spreading loss
$S_l(f)$	Signal's power spectrum at the transmitter

$H_p(t, f)$	Fourier transform, or frequency response, of $h_p(t, \tau)$
$\gamma_p(t, f)$	Small-scale scattering coefficient of the pth path bundle
S_p	Number of micropaths
P	Number of channel paths
λ	Stretching exponent of the stretched exponential function
$f(t, \tau)$	The lowpass impulse response of the equivalent channel, $:= g(t) * c(t, \tau) * g^*(-t)$
ℓ	The discrete-time delay dispersion or spread of each path
L	The discrete-time delay spread, which is the maximum value of ℓ
$f[m, \ell]$	The time-variant FIR filter of the equivalent channel
$a_{p,i}$	Doppler scaling factor of the pth path for the ith OFDM block
T'	Duration of the OFDM block, $:= T + T_{cp}$
W_N	The primitive nth root of unity, $:= e^{-j2\pi/N}$
V_i	Doppler shift coefficient of the ith OFDM block $:= e^{j2\pi a_i f_c T_s}$
$\tilde{\epsilon}_i$	The estimated carrier frequency offset of the ith OFDM block, which is approximately the residual Doppler shift
$u_i(t)$	The ith received OFDM signal after Doppler compensation
$F_{\mathcal{C}}(\nu)$	Cumulative distribution function of $S_C(\nu)$
$\mathrm{E}[\cdot]$	Expected value
$\mathcal{H}$	The random variable of $h(t, \tau)$
$\mathcal{C}$	The random variable of $c(t, \tau)$
$\mathbf{x}$	Transmitted baseband signal vector
$\mathbf{n}$	Passband noise vector
$\mathbf{z}$	Filtered baseband noise vector
$\mathbf{y}$	Received baseband signal vector

$\mathbf{F}$	The unitary discrete Fourier transform matrix
$\mathbf{C}_f$	Lowpass equivalent channel matrix
$\mathbf{C}_f^{(f)}$	Diagonalized matrix of the DFT of $\mathbf{C}_f$
$\mathbf{V}_i$	The Doppler shift diagonal matrix with components $\{V_i\}$

Acknowledgements

Chapter 1

Introduction

1.1 Background and Motivation

Underwater channels are one of the most complicated channels to work with in a communications system, and for various reasons. One reason is the severe frequency-selective fading present in the channel, that is, the dispersion (spread) in the channel exceeds the duration of the transmitted signal. This translates into rapid oscillations in the frequency response of the channel within the range of frequencies of the transmitted signal.

Though the channel is generally frequency-selective, certain assumptions about the channel can be made which allow modelling the channel as a flat fading (or narrowband) channel, i.e. the duration of the transmitted signal exceeds the dispersion in the channel, though this is not always the case. The OFDM modulation scheme however offers a solution to this problem, and provides reliable transmission over such channels. This is because the signal is transmitted over many subcarriers, which would result in subdividing the channel's frequency response into smaller subchannels. With enough subcarriers, the subchannels can be made small enough until the frequency response is nearly flat within the region of the subchannel.

Another reason for the complicated nature of underwater channels is that, not only does the attenuation factor vary with time, but it varies with frequency as well on each path. This is different from most other channels, where the attenuation factor either varies with time only or approximately constant.

Finally, one of the main reasons that make underwater channels complex when compared to other channels is the severe Doppler effect in the channel, which makes the channel a fast fading channel. Doppler shift is caused due to the relative motion of the transmitter and the receiver; Doppler shift can also be caused by wave motion, specifically gravity waves, which are waves generated in fluids or on an air-fluid interface due to the change in medium density along the propagation path. Because of

these gravity waves, different Doppler shifts occur on each channel path.

The Doppler broadening, or spread, is the maximum difference in the Doppler shifts of channel paths. Since the acoustic wave (or sound) propagation velocity is slow compared to the speed of light, Doppler spread (and shift) is a much more significant limitation than other communications channels, such as radio channels.

1.2   contributions

This thesis contributes to the area of underwater communications in both theory and practice. Specifically, it presents models and simulations based on well-known assumptions and theories in the field. The main contribution of the thesis is the OFDM simulators it presents, which took a significant amount of time to build, and is based on the treatment presented. The turbo-coded OFDM simulator was tested under two-path test channels and a real underwater channel, and the tests show that it has a good performance under harsh channel conditions.

The other contribution it makes is modifying the SOS model to take into account the distribution of Doppler frequencies, i.e. the Doppler power spectrum, in underwater channels. This in turn allows the use of the sum-of-sinusoids (SOS) model in OFDM simulations of underwater channels, which ultimately results in a turbo-coded OFDM simulator that runs under a randomly-generated underwater channel.

The simulators are based on the theory presented in the thesis, except for Chapter 4, due to the absence of a Doppler estimator. However Doppler estimation and compensation will be part of future work in this research.

1.3   Outline of the Thesis

This paper aims to investigate these points and more in detail and with a reasonable level of rigour. Chapter 2 provides an overview of OFDM and multipath channels and their statistical characterization. The wide-sense stationary uncorrelated scattering (WSSUS) assumption is used for the channel which allows statistical characterization of the channel with scattering functions, delay power profiles and Doppler power spectral density functions. The treatment given in the overview is general more or less and can be found in various sources such as [1, 2, 3].

Chapter 3 then discusses underwater acoustic (UWA) channel modelling. The UWA channel model is developed from first principles, with an approach similar to that in [4, 5, 6]. Thanks to the WSSUS assumption, the sum-of-sinusoids (SOS) method is used to randomly generate the time-varying taps of an equivalent discrete-time UWA channel model, which is useful for simulating UWA channels with Doppler effects [7, 8]. It shows correlated complex Gaussian channel tap statistics with Rayleigh or Rician amplitude distributions. Unlike channels such as radio channels, where the Doppler power spectrum is modelled by the Jakes' model, the Doppler power spectrum in underwater channels is modelled with a stretched exponential model [9], from which the Doppler spread can be estimated.

Chapter 4 provides a rigorous analysis of OFDM on UWA channels, with special focus on the Doppler effect in the channel [7, 10, 11, 12]. This is followed by ICI analysis and parametrization [11, 12]. Doppler compensation will then be discussed, and two methods will be presented [10, 12].

Chapter 5 will put the theoretical analysis from the previous chapters into practice by presenting the OFDM simulators designed over the course of the research. This work culminated in two main simulation models that were tested and proved to be a success. However due to absence of Doppler estimation, Doppler compensation was not included in the models. Chapter 6 will present the conclusions drawn by the author of the paper.

This research is very significant in the fields of digital communications and electrical engineering, and can have various applications in the fields of oceanography and physics. Throughout the research period, by collaborating with Ultra Electronics Maritime Systems Inc., experiments were performed and data were collected to test the models and simulations presented in this paper.

Chapter 2

OFDM and Multipath Channels: An Overview

2.1 OFDM Theory

Orthogonal Frequency-Division Multiplexing (OFDM) is frequency-division signaling with narrowly-spaced, but mutually orthogonal multiple carriers. It is a specific implementation of multi-carrier (MC) modulation. Even though the OFDM subcarriers overlap in frequency, they are orthogonal, and their required spectrum is hence smaller compared to conventional FDM.

OFDM does not require the use of expensive bandpass filters required in conventional FDM systems to isolate the carriers, but is sensitive to crosstalk, the unwanted coupling of one carrier into others, if timing errors occur or the channel undergoes rapid time variations [1, p. 696]. A decisive advantage of OFDM is that it can be modulated and demodulated with the low-complexity fast Fourier transform (FFT) algorithm. Also, the capability to equalize a frequency-selective channel by simple matrix multiplication in the frequency domain was a decisive factor in the adoption of OFDM in several new signaling standards for radio systems.

The main disadvantage of OFDM, its high peak-to-average power ratio due to the noise-like statistics of the time-domain signal, was not considered as disqualifying, since advances in linear amplifier technology have made this problem less of an obstacle. In fact, in the latest 4-th generation cellular standard, the uplink signaling format uses modified OFDM signals, specifically designed to reduce the peak-to-average power ratio and to enable cheaper amplifiers in the handsets for these systems.

OFDM works as follows: in baseband, the total channel of bandwidth W is divided into N subcarriers at frequency f_k, and the frequency spacing between subcarriers,

$$\Delta f = f_{k+1} - f_k \tag{2.1}$$

is related to the signal bandwidth W and number of subcarriers N as

$$f_k = k(W/N) \tag{2.2}$$

where $k \in [0, N-1]$. The symbol rate is

$$r = 1/T = \Delta f = W/N \tag{2.3}$$

where T is the symbol duration. Here $W = 1/T_s$ where T_s is the single-carrier symbol time, which by the sampling theorem is equal to the sample time. Thus $T = NT_s$, and $f_k = k/T$.

The inner product of two modulated waveforms with different subcarriers vanishes, verifying orthogonality:

$$\int_0^T e^{j2\pi f_l t} e^{-2\pi f_m t} dt = 0 \quad \text{where } l \neq m$$

The orthogonality of the modulated subcarriers means that N symbols can be sent separately and decoded independently of each other under ideal transmission conditions. That is, instead of sending N symbols over the channel at rate $r_s = 1/T_s = N/T = W$ as in a time-domain system, each symbol is sent over its corresponding subcarrier frequency f_k, and N symbols can be transmitted in parallel over the channel, each at rate of $r = r_s/N$.

The complex baseband signal to be transmitted at the output of an analog OFDM transmitter is thus given by

$$x(t) = \frac{1}{\sqrt{N}} \sum_{k=0}^{N-1} X[k] e^{j2\pi f_k t} = \frac{1}{\sqrt{N}} \sum_{k=0}^{N-1} X[k] e^{j2\pi kt/T}, \quad 0 \leq t \leq T \tag{2.4}$$

where $X[k]$ is the kth complex constellation point, for example a QPSK or 16-QAM signal point, and the constant $1/\sqrt{N}$ normalizes the expression. Generally, the constellation points, and hence the OFDM blocks, vary with time, i.e. they are given by $X_k(t)$ instead of $X[k]$, but the notation $X[k]$ was chosen for simplicity, with no substantial loss of generality in this and later analysis. Although the OFDM signal is time-limited, it is also approximately band-limited, since $X[k]$ is approximately zero

outside $k \in [0, N-1]$. Using the fact that $f_k = k/T = k(W/N)$ and sampling $x(t)$ at times $t \to nT_s$ yields the discrete samples

$$x[n] = \frac{1}{\sqrt{N}} \sum_{k=0}^{N-1} X[k] e^{j2\pi k(W/N)nT_s}$$

Since $T_s = 1/W$, $x[n]$ becomes

$$x[n] = \frac{1}{\sqrt{N}} \sum_{k=0}^{N-1} X[k] e^{j2\pi kn/N}, \qquad 0 \le n \le N-1 \tag{2.5}$$

which is a complex baseband time sequence.

One can observe that $x[n]$ is related to the complex sequence $X[k]$ via the inverse discrete Fourier transform, i.e., $x[n] = \text{IDFT}\{X[k]\}$. Therefore, rather than working with an analog transceiver, a digital transceiver can be used where, after mapping the discrete-time sequence, the transmitter performs an IDFT on the sequence, followed by an interpolation filter. This makes for a more efficient design of an OFDM system, both computationally and economically.

The interpolation filter is used to convert the discrete-time sequence into a continuous-time signal. A strictly bandlimiting interpolation function would use the function $\text{sinc}(x) = \sin(\pi x)/(\pi x)$, as known from the sampling theorem:

$$x(t) = \sum_{n=0}^{N-1} x[n]\text{sinc}((t - nT_s)/T_s)$$

However, the $\text{sinc}(x)$ interpolation pulse has significant pre-, and post-cursors and can easily generate intersymbol interference unless a large guard band is used. It is also difficult to generate with limited effort. Practically, a filter $g(t)$ like a root-raised-cosine filter with an appropriately small roll-off factor α, or other appropriate low-pass transmission filter, is used to avoid excessive temporal sidelobes. Thus

$$x(t) = \sum_{n=0}^{N-1} x[n]g(t - nT_s) = \sum_{n=0}^{N-1} x[n]g(t - nT/N) \tag{2.6}$$

After interpolation the baseband signal can be upconverted to a real, passband signal. The passband OFDM signal $s(t)$ is generated from the equivalent complex baseband signal $x(t)$ as

$$s(t) = \text{Re}\{x(t)e^{j2\pi f_c t}\} = x_i(t) \cos 2\pi f_c t - x_q(t) \sin 2\pi f_c t \qquad (2.7)$$

where the real and imaginary components, $x_i(t)$ and $x_q(t)$, are the in-phase and quadrature components of $x(t)$ respectively. f_c is a carrier frequency offset, or also the first frequency in the OFDM band. If the signal is transmitted on the passband through the channel, the received signal is downconverted first before passing through the root-raised-cosine filter at the receiver.

Assume that signal transmission is on the baseband. Let the received signal be $y(t)$ and the AWGN be $n(t)$. $y(t)$ is sampled at the output of the receive filter $g^*(-t)$ to convert the continuous signal back to discrete samples at the receiver. Due to the matched filtering process, for an AWGN channel, $y(t)$ is related to the input symbols through

$$y(t) = \sum_{n=0}^{N-1} x[n]q(t - nT/N) + z(t) \qquad (2.8)$$

where $q(t) = g(t) * g^*(-t)$ and $z(t) = n(t) * g^*(-t)$. Because $q(t)$ satisfies the Nyquist criterion for no inter-symbol interference (ISI) – or inter-sample interference in this case – that is,

$$q(nT) = \begin{cases} 1, & \text{if } n = 0, \\ 0, & \text{if } n \neq 0 \end{cases}$$

there will be no ISI at the receiver. Therefore $y(t) = x(t) + z(t)$ and the sample values $y[n]$ obtained at the receiver are given as

$$y[n] = x[n] + z[n]$$

These values can be directly applied to the FFT to retrieve the data $X[k]$.

For a multipath channel, however, inter-carrier interference, or ICI, also needs to be eliminated. In slow fading channels ICI can be eliminated with a cyclic prefix (CP). The CP is inserted prior to interpolation and transmission, which is a prefix copy of a portion of the transmitted sequence $x[n]$. However the main advantage of the CP is that it allows the linear convolution to be implemented as a circular convolution, but the CP length needs to satisfy a certain condition first.

Let the length of the discrete-time multipath channel $h[n]$ be M, and let the length of the CP be N_{cp}. To implement the linear convolution operation as a circular convolution, the CP length must satisfy the condition $N_{cp} \geq M-1$, before the samples of the CP are removed after filtering and decimation at the receiver. If $N \gg N_{cp}$ as in the usual case, the rate loss due to CP addition is minimal.

After CP removal, the length of the received sequence is N. Now by the circular convolution theorem, the circular convolution in the n domain is translated to a product in the k domain. The output of the FFT processor is now influenced by the tapped delay line equivalent channel that results from the sampling process, and each frequency is multiplied by a complex gain factor, i.e.,

$$Y[k] = H[k]X[k] + Z[k] \quad \text{where } 0 \leq k \leq N - 1$$

The output samples in the time domain, after adding the CP, are given in vector form as

$$\boldsymbol{y} = \mathbf{H}\boldsymbol{x} + \boldsymbol{z} \tag{2.9}$$

where

$$\mathbf{H} = \begin{bmatrix} h_0 & & & & h_{M-1} & \cdots & h_1 \\ \vdots & h_0 & & & & \ddots & \vdots \\ \vdots & \vdots & \ddots & & & & h_{M-1} \\ h_{M-1} & \vdots & \ddots & h_0 & & & \\ & h_{M-1} & \ddots & \vdots & h_0 & & \\ & & \ddots & \vdots & \vdots & \ddots & \\ & & & h_{M-1} & h_{M-2} & \cdots & h_0 \end{bmatrix} \tag{2.10}$$

Due to CP addition, $\mathbf{H}$ is an $N \times N$ circulant matrix. In the frequency domain, the Fourier transform diagonalizes a circulant matrix and the frequency-domain expression is obtained as

$$\boldsymbol{Y} = \mathbf{H}^{(f)}\boldsymbol{X} + \boldsymbol{Z} \tag{2.11}$$

where

$$\mathbf{H}^{(f)} = \begin{bmatrix} H[0] & & \\ & \ddots & \\ & & H[N-1] \end{bmatrix} \tag{2.12}$$

The vector $\boldsymbol{y} = [y[0] \cdots y[N-1]]^T$ thus has components

$$y[n] = \frac{1}{\sqrt{N}} \sum_{k=0}^{N-1} H[k]X[k]e^{j2\pi kn/N} + z[n] \tag{2.13}$$

and this discrete sequence of samples is demodulated by the FFT into

$$Y[k] = \frac{1}{\sqrt{N}} \sum_{n=0}^{N-1} y[n]e^{-j2\pi kn/N} = H[k]X[k] + Z[k] \tag{2.14}$$

To compensate for the channel distortion and recover $X[k]$, in general, a filter $H_f(e^{j\omega})$ (the discrete-time Fourier transform of $h[n]$) is required whose frequency response is the reciprocal of the channel's frequency response, that is, a filter with $H_f(e^{j\omega}) = 1/H(e^{j\omega})$. Instead of introducing this filter before the FFT, more typically one equalizes in the digital domain by scaling the values $Y[k]$ as $Y[k]/H[k] = X[k] + Z[k]$. Therefore the output of the filter, disregarding noise, equals $X[k]$ and is free of channel frequency gain distortion. With noise, the filter outputs will actually be the least-square estimates of $X[k]$, designated by $\tilde{X}[k]$. After finding the DFT values $\tilde{X}[k]$, which are the received constellation points of the input data, the data signal is demapped into the information-bit sequence. This allows retrieving the data.

2.2 Multipath Channels

A multipath channel is in general a linear time-varying filter channel. For an upconverted input $s(t)$, the channel's output in the passband is given by

$$r(t) = s(t) * h(t, \tau) + n(t) \tag{2.15}$$

where $n(t)$ is additive noise and $h(t, \tau)$ is the bandpass impulse response of the channel.

If an impulse is transmitted through a time-varying multipath channel, the received signal may appear as a train of impulses, which shows that time-dispersion (or time-spreading) is one of the characteristics of a multipath channel. Another characteristic is due to the time variations occurring within the channel, which means that the multipath channel varies with time, causing the train of impulses received to be different every time an impulse is transmitted [2, p. 831]. It follows that there can be different path delays and a different number of impulses received each time, and the impulses can also be attenuated differently each time.

Assuming a time-varying attenuation factor (or path gain) $h_p(t)$ and a time-variant propagation delay $\tau_p(t)$, the passband channel output signal $r(t)$ can then generally be given by

$$r(t) = \sum_p h_p(t) s[t - \tau_p(t)] + n(t) \tag{2.16}$$

where p represents the pth path (for the case of acoustic channels however, the attenuation factor is also frequency-dependent; see section 3.1). The bandpass impulse response of the channel is therefore given by

$$h(t, \tau) = \sum_p h_p(t) \delta[\tau - \tau_p(t)] \tag{2.17}$$

Using the fact that a passband signal $s(t) = \text{Re}\{x(t) e^{j2\pi f_c t}\}$ where $x(t)$ is its baseband equivalent, $r(t)$ can be written as

$$r(t) = \text{Re}\left\{ \sum_p h_p(t) x[t - \tau_p(t)] e^{j2\pi f_c [t - \tau_p(t)]} \right\} + n(t)$$

Now the baseband equivalent of the channel output $r(t)$ is given by

$$y(t) = \sum_p h_p(t)e^{j\theta_p(t)}x[t - \tau_p(t)] + \tilde{n}(t) \tag{2.18}$$

where $\theta_p(t) = -2\pi f_c \tau_p(t)$ and $\tilde{n}(t)$ is the noise signal in the baseband. Therefore the lowpass impulse response of the channel is

$$c(t, \tau) = \sum_p h_p(t)e^{j\theta_p(t)}\delta[\tau - \tau_p(t)] \tag{2.19}$$

It should be noted that $h_p(t)$ changes significantly with time only if there are large dynamic changes in the channel. However from the definition of $\theta_p(t)$ it is seen that $\theta_p(t)$ can change by 2π rad as $\tau_p(t)$ changes by $1/f_c$. Since f_c is usually large, $1/f_c$ is small, and so $\theta_p(t)$ changes rapidly. Changes in $\tau_p(t)$ are independent for different paths. $c(t, \tau)$ is often modelled as a random process, and for a large number of paths, using the central limit theorem, $c(t, \tau)$ can be approximated as a complex-valued Gaussian random process (it follows that $y(t)$ can also be modelled as such). The random variable of the envelope $|c_p(t)|$, which is equivalent to $|h_p(t)|$, can be Rayleigh, Rician, Nakagami, etc.

Let the R.V. representing $|h_p(t)|$ be $|\mathcal{H}_p|$. Assuming that no LOS (line-of-sight) is present, a Rayleigh distribution for $|\mathcal{H}_p|$ can be assumed. The Rayleigh PDF of $|\mathcal{H}_p|$ is given by

$$p(|h_p|) = \frac{|h_p|}{\sigma^2}e^{-\frac{|h_p|^2}{2\sigma^2}} \tag{2.20}$$

with mean and variance given by

$$\mathrm{E}[|\mathcal{H}_p|] = \sigma\sqrt{\frac{\pi}{2}} \tag{2.21}$$

$$\mathrm{VAR}[|\mathcal{H}_p|] = \left(2 - \frac{\pi}{2}\right)\sigma^2 \tag{2.22}$$

Throughout the research period, $|\mathcal{H}_p|$ and $|\mathcal{C}_p|$ (the R.V. of $|c_p(t)|$) were assumed to be Rayleigh-distributed, and the R.V. of the phase $\theta_p(t)$ was assumed to be uniformly distributed in $[0, 2\pi)$ or $[-\pi, \pi)$. The SOS (sum-of-sinusoids) model, which is discussed in section 3.2, is based on these assumptions.

Fading is a result of time variation in $\theta_p(t)$, the phase of each path. This random time variation in the phases can cause constructive or destructive interference of the vectors $h_p(t)e^{j\theta_p(t)}$. Constructive interference causes the received signal to appear amplified while destructive interference causes it to "fade" out [2, p. 833]. Thus signal fading (the variations in $h_p(t)e^{j\theta_p(t)}$) is due to time-variant multipath effects of the channel.

2.3 Statistical Description

Assume that $c(t, \tau)$ is wide-sense stationary, that is, the second-order moments of the channel are stationary. Mathematically, this is written as

$$E[c(t, \tau)] = m_c(\tau) \tag{2.23}$$

$$R_c(t_1, t_2, \tau_1, \tau_2) = R_c(t_2 - t_1, \tau_1, \tau_2) = R_c(\Delta t, \tau_1, \tau_2) \tag{2.24}$$

where $m_c(\tau)$ is the mean value of the channel's impulse response and $R_c(t_1, t_2, \tau_1, \tau_2)$ is the autocorrelation function of the channel's impulse response. The time difference is $\Delta t = t_2 - t_1$. Hence the autocorrelation function under the WSS assumption can be defined as

$$R_c(\Delta t, \tau_1, \tau_2) = E[c(t, \tau_1)c^*(t + \Delta t, \tau_2)] \tag{2.25}$$

Assume also uncorrelated scattering in the channel, that is, the channel's attenuation and phase shift at path delay τ_1 are uncorrelated with those at τ_2. Therefore under uncorrelated scattering, $R_c(\Delta t, \tau_1, \tau_2) = R_c(\Delta t, \tau)\delta(\tau_2 - \tau_1)$ where τ can either be τ_1 or τ_2 [2, p. 834].. This is the WSSUS (wide-sense stationary uncorrelated scattering) assumption, and throughout the research period, the WSSUS assumption was applied to the channel. This allows the use of the SOS model, which is discussed in section 3.2.

Letting $\Delta t = 0$, $R_c(\Delta t, \tau) = R_c(\tau)$, which gives the average power output of the channel as a function of path delay, and is known as the channel's multipath intensity profile, or the delay power spectrum. The range of values of τ for which $R_c(\tau) \neq 0$ is known as the channel's multipath (or delay) spread, T_m. Thus T_m can be defined as

the maximum difference in the path delay of each path:

$$T_m = \max\{|\tau_p - \tau_q|\}, \quad \forall p, q \tag{2.26}$$

where τ_p is the pth path delay and τ_q is the qth path delay.

Alternatively, the channel characterization can also be done in the frequency domain. Let $C(t, f)$ be the Fourier transform of $c(t, \tau)$ in the τ variable. If $c(t, \tau)$ is assumed to be a complex-valued Gaussian random process, then $C(t, f)$ will also be Gaussian. Since a wide-sense stationary channel is assumed, the channel's autocorrelation function is

$$R_C(\Delta t, f_1, f_2) = E[C^*(t, f_1)C(t + \Delta t, f_2)] \tag{2.27}$$

For uncorrelated scattering, using the relation between $R_C(\Delta t, f_1, f_2)$ and $R_c(\Delta t, \tau_1, \tau_2)$, and Fourier transform properties, one of the transforms collapes, and $R_C(\Delta t, f_1, f_2) = R_C(\Delta t, \Delta f)$, where $\Delta f = f_2 - f_1$ is the frequency spacing. $R_C(\Delta t, \Delta f)$ is known as the channel's spaced-frequency, spaced-time correlation function. Letting $\Delta t = 0$, $R_C(\Delta t, \Delta f)$ becomes the spaced-frequency correlation function $R_C(\Delta f)$, which is wide-sense stationary in the frequency variable f.

The channel's coherence bandwidth B_{coh} can be approximated as the inverse of the delay spread $1/T_m$, meaning that two signals with a frequency separation greater than B_{coh} will be affected independently by the channel. A channel is frequency-selective (or wideband) if $T_m > T$ or $B_{coh} < W$ (T is the signal's duration and W is the signal's bandwidth); this means that the transmitted signal will be perceptibly distorted by the channel. If $T_m \ll T$ or $B_{coh} \gg W$ then the channel is frequency-nonselective, or flat (also called narrowband).

In underwater acoustic communications, or UWA communications for short, large channel multipath spreads occur due to the relatively small speed of sound waves (around 1500 m/s in water) and the presence of multipath in the channel; this leads to severe ISI due to the dispersion (or spreading) of the waveform in time. In shallow water, the multipath spread is usually in the order of tens of milliseconds, but sometimes it can be as large as 100 ms. In deep water, the multipath spread is in the order of seconds [10, p. 8]. A large multipath spread also results in a small coherence

bandwidth. Thus the UWA channel is a frequency-selective, or wideband, channel.

The next focus will now be on the channel's time variations which are due to Doppler broadening (or Doppler spread) and also possibly to Doppler shift. The Doppler effects are characterised by the scattering function $S_C(\nu, \Delta f)$, which is the Fourier transform of $R_C(\Delta t, \Delta f)$.

If $\Delta f = 0$, then $S_C(\nu)$ is the channel's Doppler power spectrum, which gives the average power output of the channel per unit Doppler frequency. The range of values of ν for which $S_C(\nu) \neq 0$ is the channel's Doppler spread, which measures Doppler broadening, and is given by B_d. Thus B_d is defined as the maximum difference in the Doppler frequency of each path:

$$B_d = \max\{|\nu_p - \nu_q|\}, \quad \forall p, q \tag{2.28}$$

where ν_p is the Doppler frequency of the pth path and ν_q is the Doppler frequency of the qth path. Doppler spread may also be defined as the 3-dB bandwidth of each path's Doppler power spectrum [2, p. 837]. Doppler spread typically varies with the path time delay.

Making use of the relationship between $R_c(\Delta t)$ and $S_C(\nu)$, the channel's coherence time T_{coh} can be approximated by $1/B_d$. Here the following classification can be made: if $T_{coh} \gg T$ or $B_d \ll W$ then the channel is slowly changing and the channel is called a slow fading channel. If $T_{coh} < T$ or $B_d > W$ then the channel is a fast fading (or time-selective) channel.

In UWA communications, large channel Doppler shifts and spreads occur due to the relatively small speed of sound. In MC modulation, this leads to severe ICI due to the dispersion (or spreading) of the waveform in frequency [10, p. 9]. A large Doppler spread also results in a small coherence time. Thus the UWA channel is a fast fading, or time-selective, channel.

The properties of the autocorrelation function discussed in this section can be used to yield alternative definitions for the WSSUS model. Using the relation between $S_C(\nu_1, \nu_2, f_1, f_2)$ and $R_c(t_1, t_2 \tau_1, \tau_2)$, and Fourier transform properties, the WSS assumption yields

$$S_C(\nu_1, \nu_2, f_1, f_2) = S_C(\nu, f_1, f_2)\delta(\nu_2 - \nu_1) \tag{2.29}$$

(where ν can either be ν_1 or ν_2). Therefore, the WSS assumption is the assumption of uncorrelated scattering of Doppler frequencies. Alternatively, using the relation between $R_c(t_1, t_2, \tau_1, \tau_2)$ and $S_C(\nu_1, \nu_2, \tau_1, \tau_2)$, using Fourier transform properties, and finally invoking the WSSUS assumption yields the statements

$$S_C(\nu_1, \nu_2, \tau_1, \tau_2) = S_C(\nu, f)\delta(\nu_2 - \nu_1)\delta(\tau_2 - \tau_1) \tag{2.30}$$

$S_C(\nu, \tau)$ is the scattering function of the channel, which gives the average power output of the channel as a function of ν and τ.

Chapter 3

UWA Channel Modelling

3.1   The UWA Channel

One of the main factors that characterize acoustic propagation is frequency-dependent attenuation. The channel's impulse response can be sparse, and it is modelled as a linear time-variant (low-pass) filter. In UWA channels, signals are transmitted at low frequencies, mainly due to the frequency dependence of the channel's attenuation factor. UWA channels are also frequency-selective fading (wideband) channels, and sparse channel estimation is used to improve performance in such a channel. The analysis and modelling of the UWA channel, and the formulation of the channel's impulse response $h(t, \tau)$ presented in this section are widely used by researchers today. The discussion presented here is closely related to the work done by Stojanovic in [4, 5, 6].

The attenuation factor of the channel is frequency-dependent due to absorption, i.e. the transfer of acoustic (sound) energy into heat. As known from physics, the average power transferred by sound travelling through a constant cross-section is $\frac{1}{2}\rho v \omega^2 A s_{max}^2$ where s_{max} is the maximum displacement amplitude of the wave, ρ is the density of the propagation medium, v is the wave speed, A is the cross-sectional area through which the wave propagates and ω is the angular frequency of the wave. Therefore, since the path loss (and hence the attenuation factor) is related to the power transferred, it is frequency-dependent.

Furthermore, there is spreading loss which increases with distance, which is the energy loss due to the scattering of the waves in a specific geometry. Thus the path (propagation) loss is also distance-dependent. The path loss is given by the equation [4]

$$A(l, f) = (l/l_r)^\kappa [a(f)]^{l-l_r} \tag{3.1}$$

where l is the distance between the transmitter and receiver (transmission distance),

l_r is the reference distance, and $a(f)$ is the absorption coefficient. κ is the path loss exponent that models the spreading loss, and usually $1 \leq \kappa \leq 2$ (1 is for cylindrical spreading and 2 is for spherical spreading). For frequencies up to about 50 kHz, the logarithm of the absorption coefficient has a second-order approximation [4]:

$$10 \log a(f) \approx \alpha_0 + \alpha_1 f + \alpha_2 f^2 \tag{3.2}$$

(the transceiver design, which is discussed in a later section, operates around the frequency of 2 kHz).

Effects of path loss can also be seen on the signal-to-noise ratio. Due to path loss, the transmitted signal power is degraded to $S_l(f)/A(l, f)$ where $S_l(f)$ is the power spectrum of the signal at the transmitter (the subscript l shows that the signal power can be modified with distance). Noise in acoustic channels is made of ambient noise and noise from other surrounding sources (like turbulence and ships), however the ambient noise is not white, although it is still modelled as a Gaussian random process. The noise power (or its power spectrum) is given by $N(f)$.

The distance and frequency-dependent SNR under path loss is thus given by

$$SNR(l, f) = \frac{S_l(f)}{A(l, f)N(f)} \tag{3.3}$$

Since $S_l(f)$ is usually user-specified prior to transmission, the distance and frequency dependence of the SNR comes from the factor $[A(l, f)N(f)]^{-1}$. This means that the bandwidth will depend on transmission distance, since as distance increases, the SNR decreases, causing a decrease in the channel bandwidth. Conversely, transmitting at shorter distances will give a higher SNR, and hence, a larger channel bandwidth (however transducer limitations will result in a maximum possible bandwidth that can be reached). Therefore bandwidth-efficient modulation schemes are important to achieve spectral efficiency greater than 1 bps/Hz [4].

To achieve a certain SNR, the bandwidth and power required as a function of distance can, respectively, be modelled by [5]:

$$W(l) = wl^{-\beta} \qquad \text{where} \quad \beta = 0, 1 \tag{3.4}$$

$$P(l) = pl^{\psi} \qquad \text{where} \quad \psi \geq 1 \tag{3.5}$$

($\beta = 0$ for the case of no path loss). It is important to note that since the channel's bandwidth is on the order of its carrier or center frequency, which is usually small, UWA channels are intrinsically frequency-selective.

Multipath propagation underwater is due to the reflection and refraction of the acoustic waves. Refraction is due to the change in sound speed with depth, which is significant mainly in deep water, while reflection can be at the surface and bottom of the water, and at objects in the water. Figure 3.1 below shows an illustration of this [7, p. 2]. In shallow water, the speed of sound v is almost constant, and so the path
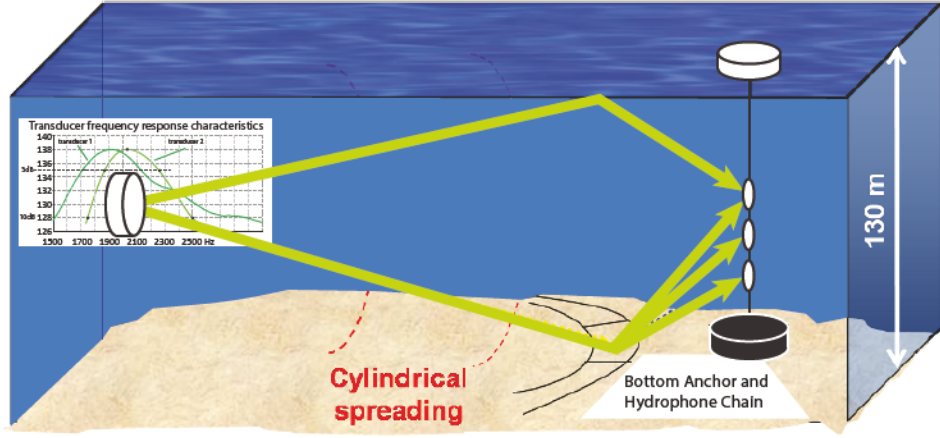

Figure 3.1: Multipath propagation in underwater environments.

delays can be computed as l_p/v, where p denotes the pth path, and the propagation path lengths can be geometrically calculated. The relative path delays $\tau_p = l_p/v - t_0$ can be defined, where t_0 is the arrival time of the path with the highest energy, which is then used as the receiver's reference time. Under motion or Doppler effects, l_p, and hence τ_p, will vary with time.

The path's total reflection coefficient is denoted by Γ_p. Under ideal conditions the reflection coefficient at the top (water) surface is -1, but the reflection coefficient at the bottom surface depends on the surface itself and the wave's incident angle on that surface. The reflection coefficient yields the channel's attenuation factor, but the path loss should also be accounted for. The frequency-dependent attenuation factor (or the frequency response of the pth path) is therefore given by [4]:

$$H_p(t, f) = \frac{\Gamma_p}{\sqrt{A(l_p, f)}} \tag{3.6}$$

(path loss is a coefficient of power loss; since the attenuation factor is a factor of energy loss, the attenuation factor would hence be reduced by $\sqrt{A(l_p, f)}$). The above model shows that dispersion occurs at each path, and each path behaves like a low-pass filter.

The Fourier transform of such a channel, $H(t, f)$, is thus given by

$$H(t, f) = \sum_p H_p(t, f)e^{-j2\pi f \tau_p(t)} \tag{3.7}$$

Hence when inverted back to the time domain, the bandpass impulse response of the channel now becomes $h(t, \tau)$, and is given by

$$h(t, \tau) = \sum_p h_p[t, \tau - \tau_p(t)] \tag{3.8}$$

where $h_p(t, \tau)$ is the inverse Fourier transform of $H_p(t, f)$. The transmitted passband signal is given by $s(t) = \text{Re}\{x(t)e^{j2\pi f_c t}\}$. The received passband signal is given by $r(t) = s(t) * h(t, \tau) + n(t)$. The received baseband signal can then be written as $y(t) = x(t) * c(t, \tau) + \tilde{n}(t)$, where

$$C(t, f) = \sum_p H_p(t, f)e^{j\theta_p(t)}e^{-j2\pi f \tau_p(t)} \tag{3.9}$$

and $\theta_p(t) = -2\pi f_c \tau_p(t)$. Letting $C_p(t, f) = H_p(t, f)e^{j\theta_p(t)}$, the equivalent lowpass response can thus be written as

$$c(t, \tau) = \sum_p c_p[t, \tau - \tau_p(t)] \tag{3.10}$$

where $c_p(t, \tau) = h_p(t, \tau)e^{j\theta_p(t)}$.

A simpler model of a multipath channel's impulse response is discussed in section 2.2:

$$h(t, \tau) = \sum_p h_p(t)\delta[\tau - \tau_p(t)]$$

$$c(t, \tau) = \sum_p h_p(t)e^{j\theta_p(t)}\delta[\tau - \tau_p(t)]$$

It is of interest sometimes to simplify the acoustic model to the form shown above. This is possible if it is assumed that the pulses of the path's delay response are narrow enough to be considered impulses. This assumption is valid if the signal's duration is significantly larger than the channel's multipath spread, i.e. the OFDM signal's bandwidth is significantly smaller than the channel's coherence bandwidth.

In other words, it is necessary to assume a flat fading channel in order to use the simplified model. But as previously discussed, the UWA channel is a frequency-selective fading channel. In OFDM however, this assumption can be valid and can often easily occur.

If the subcarrier signal's bandwidth is small enough such that the channel's frequency response is almost flat or constant in the domain of that bandwidth (which is equivalent to a coherence bandwidth much larger than the subcarrier signal's bandwidth), then the flat fading model for each signal, or symbol, in the OFDM block can be assumed, and serves as a good approximation to the UWA channel. The number of subcarriers should be large enough for this condition to be satisfied. For this reason, throughout the research period, this simplified form of the UWA channel model was assumed.

However, as seen in section 4.1, when Doppler effects are taken into account, the assumption of a narrowband problem will not hold anymore due to the Doppler shift present, which will effectively make the signal's bandwidth comparable to the coherence bandwidth and the channel will go back to being a wideband problem. Doppler compensation though will convert the problem back to a narrowband problem (see section 4.3).

The channel model for UWA systems can, in case scattering occurs along paths, also take into account path bundles, which are a spreading and scattering of the original multipath signal around the main path, due to reflection off of a rough surface. Each path bundle p is made of closely-spaced micropaths which together cause the fading effect on the path bundle. To account for the path bundles, a time-varying small-scale scattering coefficient $\gamma_p(t, f)$ should be included in the channel model for each path bundle [6].

$\gamma_p(t, f)$ is defined as the normalized sum of each micro-path response in a path bundle. Based on this definition $\gamma_p(t, f)$ can be mathematically represented as shown in [6]:

$$\gamma_p(t, f) = \frac{1}{h_p}[h_{p,0} + \sum_{\iota=1}^{S_p-1} h_{p,\iota}e^{-j2\pi f\delta_\iota(t)}] \tag{3.11}$$

ι denotes the ιth micropath in a path bundle, $h_{p,\iota}$ denotes the micropath response amplitude and $\delta_\iota(t)$ denotes the micropath delay, i.e., the delay from the main path. $h_{p,0}$ is the response amplitude of the main path, and so $\delta_0(t) = 0$.

For time durations that are much larger than the symbol duration, $\gamma_p(t, f) \approx 1$ and the previous channel model is used. However on the small-scale the effect of the micropaths becomes significant, and a path's bandpass frequency response in this model is represented by $H'_p(t, f) = H_p(f)\gamma_p(t, f)$ [6]. The channel's bandpass frequency response is therefore refined to

$$H(t, f) = \sum_p H_p(f)\gamma_p(t, f)e^{-j2\pi f\tau_p(t)} \tag{3.12}$$

and the lowpass frequency response is given by

$$C(t, f) = \sum_p C_p(f)\gamma_p(t, f)e^{-j2\pi f\tau_p(t)} \tag{3.13}$$

3.2   The SOS Model

The UWA channel can be simulated using the sum-of-sinusoids (SOS) model. As shown before, the lowpass impulse response of the UWA channel can be modelled as

$$c(t, \tau) = \sum_p c_p(t)\delta[\tau - \tau_p(t)]$$

where $c(t, \tau)$ is the lowpass time-varying impulse response and $c_p(t) = h_p(t)e^{j\theta_p(t)}$. Given that the coherence bandwidth is less than the OFDM signal's bandwidth, such a channel is frequency-selective. The time-varying channel tap $c_p(t)$ however, which is also interpreted as the impulse response of each path as seen in section 3.1, is assumed

to follow a flat-fading channel model, and so the R.V. of $|c_p(t)|$, $|\mathcal{C}_p|$, is assumed to be Rayleigh-distributed.

The SOS model states that, under 2-D isotropic (or uniform) scattering, the flat-fading channel $c(t)$ whose envelope is Rayleigh-distributed is given by [7]

$$c(t) = \frac{1}{\sqrt{P}} \sum_{p=1}^{P} e^{j(2\pi\nu_p t + \theta_p)} \tag{3.14}$$

where P is the number of propagation paths that the channel is composed of and θ_p is the uniformly-distributed random phase of the pth path in $[0, 2\pi)$ or $[-\pi, \pi)$. $\nu_p = \nu_d \cos\alpha_p$ is the Doppler frequency, where ν_d is the maximum Doppler frequency and α_p is the angle of arrival of the pth path, uniformly distributed in $[0, 2\pi)$ or $[-\pi, \pi)$; thus ν_p is uniformly (cosine) distributed in $[-\nu_d, \nu_d)$.

The scaling factor $\frac{1}{\sqrt{P}}$ ensures that $|c(t)|^2$ is normalized, i.e. $\max\{|c(t)|^2\} = 1$, and ensures convergence as $P \to \infty$ by the central limit theorem. It can be shown that as $P \to \infty$, $|\mathcal{C}|$ is Rayleigh-distributed and the R.V. of the phase $\arg\{\mathcal{C}\}$ is uniformly distributed on $[0, 2\pi)$ or $[-\pi, \pi)$. In practice P is finite, which means that the model in a strict sense is non-stationary. However, in practice the value of P is enough for the model to be an accurate representation, and even moderate values of P can produce channels close to the WSSUS channel. In discrete time, the SOS model is given by

$$c[n] = \frac{1}{\sqrt{P}} \sum_{p=1}^{P} e^{j(2\pi\nu_p nT_s + \theta_p)} \tag{3.15}$$

The frequency-selective UWA channel can also be modelled with the SOS model. Comparing $c(t)$ with $c(t, \tau)$, it follows that $c(t, \tau)$ can be modelled as [8]

$$c(t, \tau) = \frac{1}{\sqrt{P}} \sum_{p=1}^{P} e^{j(2\pi\nu_p t + \theta_p)} \delta[\tau - \tau_p(t)] \tag{3.16}$$

where

$$c_p(t) = \frac{1}{\sqrt{P}} e^{j(2\pi\nu_p t + \theta_p)} \tag{3.17}$$

However, as mentioned in section 3.1, in small-scale analysis when the time durations of transmission are on the order of the symbol duration of the signal, the effect of the

micropaths in a single path bundle needs to be accounted for. Hence in this case, the SOS model for $c_p(t)$ becomes

$$c_p(t) = \frac{1}{\sqrt{S_p P}} \sum_{\iota=1}^{S_p} e^{j(2\pi\nu_{p,\iota}t+\theta_{p,\iota})} \tag{3.18}$$

and thus

$$c(t,\tau) = \frac{1}{\sqrt{S_p P}} \sum_{p=1}^{P} \sum_{\iota=1}^{S_p} e^{j(2\pi\nu_{p,\iota}t+\theta_{p,\iota})} \delta[\tau - \tau_p(t)] \tag{3.19}$$

The factor $\frac{1}{\sqrt{S_p P}}$ ensures that $|c(t,\tau)|$ is normalized, and ensures convergence as $P \to \infty$ (by the central limit theorem). Analogous to the no-micropath case, $\theta_{p,\iota}$ is the uniformly-distributed random phase for the ιth micropath of the pth path bundle in $[0, 2\pi)$ or $[-\pi, \pi)$. $\nu_{p,\iota} = \nu_d \cos\alpha_{p,\iota}$ is the Doppler frequency, where ν_d is the maximum Doppler frequency and $\alpha_{p,\iota}$ is the angle of arrival for the ιth micropath of the pth path bundle, uniformly distributed in $[0, 2\pi)$ or $[-\pi, \pi)$; thus $\nu_{p,\iota}$ is uniformly (cosine) distributed in $[-\nu_d, \nu_d)$.

So far the model as it is assumes uniform distribution on ν_p without any regard to its relationship with the UWA channel's Doppler power spectrum. The model thus needs to be modified in order to account for that. Various experiments and measurements, such as those shown in [9], have shown that the Doppler power spectrum in underwater environments is modelled by a stretched exponential function defined as

$$S_C(\nu) = Ae^{-(|\nu|/\upsilon)^\lambda} + \eta \tag{3.20}$$

where υ and A are scaling factors, λ is the stretching exponent, and η is the noise floor; it should also be noted that $S_H(\nu) = S_C(\nu)$ since there is no dependence on τ or f. The method of least squares is used to curve-fit the stretched exponential model to the measured data.

The Doppler power spectrum can be viewed as the PDF of the R.V. $\mathcal{C}$ from which the Doppler frequencies ν_p are drawn. The Doppler frequencies can be randomly generated from the Doppler power spectrum via the method of inverse transform sampling [7]. The inverse transform sampling method states that if Y has a uniform distribution in $[0, 1]$, and if X has a CDF F_X, then the CDF of the R.V. $F_X^{-1}(Y)$

is F_X. In other words, this method states that to generate values of the R.V. of ν, which are distributed according to the CDF of the Doppler power spectrum, a uniformly-distributed random number u in $[0, 1]$ is generated first, and then the value ν is obtained from $u = F_C(\nu)$. Therefore the random value ν can now be obtained from the CDF F_C. The CDF is obtained by integrating the stretched exponential model, i.e. $F_C(\nu) = \int_{-\infty}^{\nu} S_C(\mu)d\mu$.

As an example, consider the special case when $\lambda = 1$, i.e. the case when the Doppler power spectrum is an exponential distribution. Since the Doppler power spectrum $S_C(\nu)$ is thought of as a PDF, the scaling factor A is chosen such that $\int_{-\infty}^{\infty} S_C(\nu)d\nu = 1$. A straightforward calculation shows that $A = \frac{1}{2v}$. Thus for $\lambda = 1$, and ignoring noise floor η,

$$S_C(\nu) = \frac{1}{2v}e^{-|\nu|/v} \tag{3.21}$$

The CDF $F_C(\nu)$ can now be calculated as follows:

$$
\begin{aligned}
F_C(\nu) &= \frac{1}{2v} \int_{-\infty}^{\nu} e^{-|\mu|/v}d\mu \\
&= \begin{cases} \frac{1}{2v} \int_{-\infty}^{\nu} e^{\mu/v}d\mu, & \text{if } \nu < 0, \\ \frac{1}{2v} \int_{-\infty}^{0} e^{\mu/v}d\mu + \frac{1}{2v} \int_{0}^{\nu} e^{-\mu/v}d\mu, & \text{if } \nu > 0 \end{cases} \\
&= \begin{cases} \frac{1}{2}e^{\nu/v}, & \text{if } \nu < 0, \\ 1 - \frac{1}{2}e^{-\nu/v}, & \text{if } \nu > 0 \end{cases}
\end{aligned}
$$

Therefore,

$$F_C(\nu) = \frac{1}{2} + \frac{\text{sgn}(\nu)}{2}(1 - e^{-|\nu|/v}) \tag{3.22}$$

Setting $u = F_C(\nu)$ and inverting the function yields

$$\nu = \begin{cases} v \ln 2u, & \text{if } 0 < u \leq \frac{1}{2}, \\ -v \ln (2 - 2u), & \text{if } \frac{1}{2} < u < 1 \end{cases} \tag{3.23}$$

The bandpass channel taps can now be generated using the SOS model. The SOS channel representation in (3.18) has been modelled for use in Simulink, and then subsequently used in the OFDM system simulations discussed in chapter 5. The Simulink model is shown in Figure 3.2 below for a 2-tap channel, which can represent

the impulse response of a standard "two-impulse" model for multipath channels. The "MATLAB Function" and "MATLAB Function1" blocks shown model the time-varying gain $c_p(t)$ with a fixed programmable τ_p. Both blocks have the same code; the appendix includes the MATLAB code, written for an exponential Doppler power spectrum.
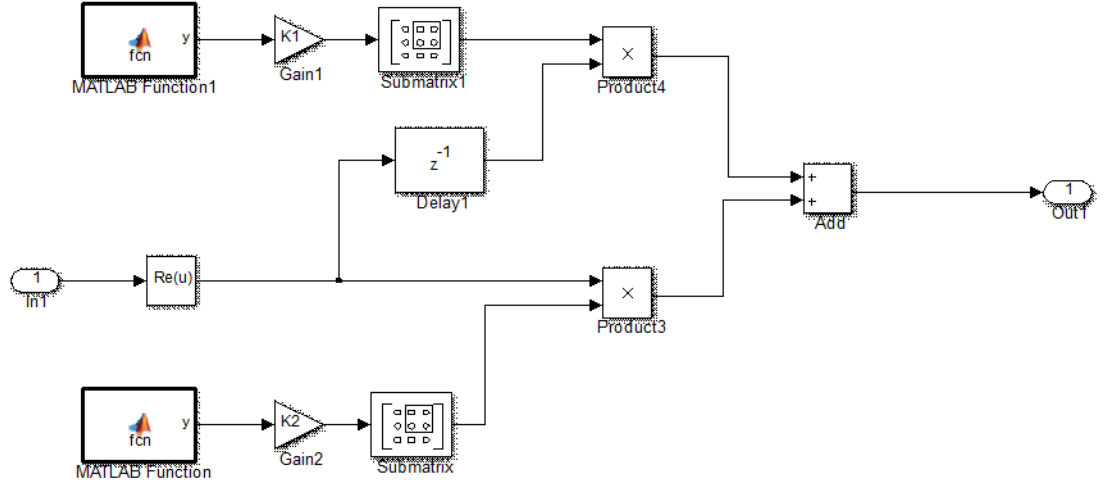

Figure 3.2: The SOS channel simulation model, shown for two taps.

The SOS model can also be constructed for the equivalent channel which includes filtering. Let the equivalent lowpass impulse response in this case be $f(t, \tau)$. If the impulse response of the transmit filter is given by $g(t)$, then the impulse response of the receive filter should be given by $g^*(-t)$. Therefore, $f(t, \tau)$ is related to $c(t, \tau)$ by

$$f(t, \tau) = g(t) * c(t, \tau) * g^*(-t) = c(t, \tau) * q(t) \tag{3.24}$$

where $q(t) = g(t) * g^*(-t)$. In large-scale analysis, where micropath effects are negligible, the SOS model for $c(t, \tau)$ is given by (3.16). It follows that the SOS model for $f(t, \tau)$ is given by [8]

$$f(t, \tau) = \frac{1}{\sqrt{P}} \sum_{p=1}^{P} e^{j(2\pi\nu_p t + \theta_p)} q[\tau - \tau_p(t)] \tag{3.25}$$

Recall that the output of the interpolation filter $g(t)$ is given by (2.6):

$$x(t) = \sum_{n=0}^{N-1} x[n]g(t - nT_s)$$

The output of the receive filter is therefore

$$y(t) = \sum_{n=0}^{N-1} x[n]f(t, t - nT_s) + z(t) \tag{3.26}$$

where $z(t) = \tilde{n}(t) * g^*(-t)$, and

$$f(t, t - nT_s) = \frac{1}{\sqrt{P}} \sum_{p=1}^{P} e^{j(2\pi\nu_p t + \theta_p)} q[t - nT_s - \tau_p(t)]$$

Now, by sampling at $t \rightarrow mT_s$, the equivalent channel is discretized to $f(mT_s, mT_s - nT_s)$, and the discrete-time filter output after CP removal is then given by

$$y[m] = \sum_{n=0}^{N-1} x[n]f[m, m - n] + z[m] = \sum_{\ell=0}^{L-1} x[m - \ell]f[m, \ell] + z[m] \tag{3.27}$$

where $\ell = m - n$, which represents the delay dispersion (spread) in each path of the channel, and $\ell \in [0, L - 1]$. This expression shows that $f[m, \ell]$ can be thought of as the time-varying tap of an FIR filter; in other words the channel is an FIR filter in discrete time, or equivalently a tapped delay line. Figure 3.3 below provides an illustration of this representation [7].

The SOS model of $f[m, \ell]$, assuming no time variations in τ_p, is given by

$$f[m, \ell] = \frac{1}{\sqrt{P}} \sum_{p=1}^{P} e^{j(2\pi\nu_p mT_s + \theta_p)} q(\ell T_s - \tau_p) \tag{3.28}$$

In small-scale analysis, the SOS model becomes

$$f(t, \tau) = \frac{1}{\sqrt{S_p P}} \sum_{p=1}^{P} \sum_{\iota=1}^{S_p} e^{j(2\pi\nu_{p,\iota} t + \theta_{p,\iota})} q[\tau - \tau_p(t)] \tag{3.29}$$

and its discrete-time representation is analogous to (3.28). Just like the model given

for the taps $c_p(t)$, θ_p is uniformly distributed in $[-\pi, \pi)$ or $[0, 2\pi)$ and ν_p is distributed according to $S_C(\nu)$. However, this model is also a function of path delay; thus the multipath intensity profile is necessary in order to generate the values of τ_p.
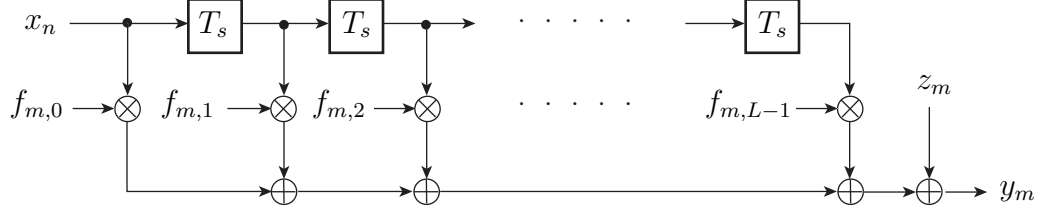

Figure 3.3: Tapped delay line model of $f(mT_s, \ell T_s) = f[m, \ell]$.

Using properties of autocorrelation functions, the expression for the multipath intensity profile $R_c(\tau)$ can be derived:

$$R_c(\tau) = \mathrm{E}[c(t, \tau)c^*(t, \tau)]$$

$$= \mathrm{E}\left[\sum_p c_p(t)\delta[\tau - \tau_p(t)] \sum_q c_q^*(t)\delta[\tau - \tau_q(t)]\right]$$

$$= \begin{cases} \sum_p \mathrm{E}\left[|c_p(t)|^2\right] \delta[\tau - \tau_p(t)] & \text{if } p = q \\ 0 & \text{if } p \neq q \end{cases}$$

Therefore,

$$R_c(\tau) = \sum_p \mathrm{E}\left[|c_p(t)|^2\right] \delta[\tau - \tau_p(t)] \tag{3.30}$$

Thus the average power of each path is $\mathrm{E}\left[|c_p(t)|^2\right]$ or $\mathrm{E}\left[|h_p(t)|^2\right]$ (since $R_c(\tau) = R_h(\tau)$). Unfortunately, unlike the Doppler power spectrum above, and unlike channels such as radio channels where the multipath intensity profile is modelled by an exponential function, the multipath intensity profile in UWA channels does not have a convenient model to generate the values of τ_p (using the impulse transform sampling method).

Chapter 4

OFDM on UWA Channels

4.1 UWA Channels and Doppler Effects

This section explores the Doppler effects present in the UWA channel. The effects of the Doppler scaling factor and Doppler shift on the OFDM signal will be shown in detail, and will be investigated for the lowpass impulse response $c(t, \tau)$ and then the equivalent lowpass impulse response $f(t, \tau)$.

From physics principles, the change in frequency due to moving platforms, or the Doppler shift, is given by $\Delta f = f_0(\Delta v_p/c)$ where f_0 is the frequency of the transmitted sound wave and Δv_p is the speed difference between the time of reception and transmission; since the gravity waves (waves generated in fluids or on an air-fluid interface due to the change in medium density along the propagation path) in water can also introduce relativistic effects, the speed difference generally varies with the path that the signal follows in the underwater environment. The factor $\Delta v_p/c$ is referred to as the Doppler scaling factor, and is commonly denoted by a_p.

Let the UWA channel be given by the time-variant channel model in (2.17). Since the UWA channel is analyzed for OFDM transmission, the channel tap $h_p(t)$, which was defined for a generic transmission scheme, is now replaced by $h_{p,i}(t)$, where i represents the ith OFDM block. Similarly, $\tau_p(t)$ is replaced by $\tau_{p,i}(t)$. The ith baseband OFDM block received is denoted by $y_i(t)$, which means that $y(t) = \sum_i y_i(t)$.

Assume that the amplitude is constant within one OFDM block, i.e. $h_{p,i}(t) = h_{p,i}$. Also assume that the delay variation of each path $\tau_{p,i}(t)$ can be approximated by the first-order linear relation $\tau_{p,i}(t) \approx \tau_{p,i} - a_{p,i}t$, where $a_{p,i}$ is the Doppler scaling factor of the pth path. These assumptions are appropriate as long as $T < T_{coh}$, which is on the order of few hundred ms at most [10, p. 12].

Also assume, and without substantial loss of generality, that the Doppler shifts are equal for all paths p, i.e., there exists one common Doppler scaling factor a_i for the ith OFDM block. This assumption is valid when the Doppler distortion due to

platform motion (transmitter and receiver) is dominant, with small variation in the angles of arrival for the paths [11]. At the transmitter each OFDM block occupies an interval $t \in [iT', (i+1)T']$ where T' is defined as $T + T_{cp}$.

Now the impulse response of the UWA channel for the ith OFDM block can be written as

$$h_i(t, \tau) = \sum_{p=1}^{P} h_{p,i} \delta[\tau - (\tau_{p,i} - a_i t)] \tag{4.1}$$

The frequency response of the channel is then given by

$$H_i(t, f) = e^{j2\pi a_i f t} \sum_{p=1}^{P} h_{p,i} e^{-j2\pi f \tau_{p,i}} = e^{j2\pi a_i f t} H_i(f) \tag{4.2}$$

which shows time- and frequency-dependent phase shifts for the different OFDM blocks. According to (2.19), the lowpass equivatent of the channel is now given by

$$c_i(t, \tau) = e^{j2\pi a_i f_c t} \sum_{p=1}^{P} h_{p,i} e^{-j2\pi f_c \tau_{p,i}} \delta[\tau - (\tau_{p,i} - a_i t)] \tag{4.3}$$

where $a_i f_c$ is the Doppler shift present in the channel. Hence the frequency response is

$$C_i(t, f) = e^{j2\pi a_i(f+f_c)t} \sum_{p=1}^{P} h_{p,i} e^{-j2\pi(f+f_c)\tau_{p,i}} = e^{j2\pi a_i(f+f_c)t} C_i(f) \tag{4.4}$$

but it can also be given in other forms like

$$C_i(t, f) = H_i(t, f + f_c) = e^{j2\pi a_i(f+f_c)t} H_i(f + f_c) \tag{4.5}$$

The passband signal received is given by

$$r_i(t) = s_i(t) * h_i(t, \tau) + n_i(t) \tag{4.6}$$

which yields

$$r_i(t) = \sum_{p=1}^{P} h_{p,i} s_i[(1 + a_i)t - \tau_{p,i}] + n_i(t) \tag{4.7}$$

Thus each OFDM block at the receiver occupies an interval $t \in [\frac{iT' + \tau_{p,i}}{1 + a_i}, \frac{(i+1)T' + \tau_{p,i}}{1 + a_i}]$.

It should be noted that since $|a_i| < 1$, $1 + a_i > 0$. Similarly, the baseband signal received can be written as

$$y_i(t) = e^{j2\pi a_i f_c t} \sum_{p=1}^{P} h_{p,i} e^{-j2\pi f_c \tau_{p,i}} x_i[(1 + a_i)t - \tau_{p,i}] + \tilde{n}_i(t) \qquad (4.8)$$

where $t \in [\frac{iT' + \tau_{p,i}}{1 + a_i}, \frac{(i+1)T' + \tau_{p,i}}{1 + a_i}]$. The Fourier transform of $y_i(t)$ (given in (4.8)) is given by

$$Y_i(f) = \frac{1}{1 + a_i} X_i \left(\frac{f - a_i f_c}{1 + a_i} \right) \sum_{p=1}^{P} h_{p,i} e^{-j2\pi \left(f_c + \frac{f}{1+a_i} \right) \tau_{p,i}} + \tilde{N}_i(f) \qquad (4.9)$$

Therefore,

$$Y_i(f) = \frac{1}{1 + a_i} C_i \left(\frac{f}{1 + a_i} \right) X_i \left(\frac{f - a_i f_c}{1 + a_i} \right) \qquad (4.10)$$

Substituting (2.4) into (4.8) gives a more useful representation of $y_i(t)$:

$$y_i(t) = \frac{1}{\sqrt{N}} e^{j2\pi a_i f_c t} \sum_{k=0}^{N-1} X[k] e^{j2\pi f_k (1 + a_i)t} \sum_{p=1}^{P} h_{p,i} e^{-j2\pi (f_c + f_k)\tau_{p,i}} + \tilde{n}_i(t)$$

This can be simplified to

$$y_i(t) = \frac{1}{\sqrt{N}} e^{j2\pi a_i f_c t} \sum_{k=0}^{N-1} C(f_k) X[k] e^{j2\pi f_k (1 + a_i)t} + \tilde{n}_i(t) \qquad (4.11)$$

A similar expression can be found in [12]. This expression is very useful for the next two sections.

From the analysis so far two effects have persisted, which are more clearly seen in equations (4.8) and (4.11). First, the signal duration from each path is scaled to $T/(1 + a_i)$ (including the CP, it is scaled by $(T + T_{cp})/(1 + a_i)$). Typically, a_i is on the order of 10^{-3} or 10^{-2} for UWA channels, and so the stretching/compression of the block duration is small. However in the frequency domain, since a large number of subcarriers is usually chosen, the ICI introduced is in most cases substantial, and needs to be compensated for (section 4.3).

Second, the frequency components in the signals experience a subcarrier-dependent Doppler shift of $a_i(f_c + f_k)$, which effectively causes the bandwidth of each subcarrier signal (or the subchannel bandwidth) to increase; consequently the narrowband

assumption breaks down, because now the channel's frequency response is no longer flat in the domain of the transmitted signal's bandwidth. Therefore, the problem at this stage goes back to being a wideband problem. Doppler compensation in section 4.3 resolves these issues.

It is also useful to express the received OFDM block in a matrix form that models $y_i(t)$ completely and more concisely than the approach above. One way to do this is the following. Substituting (2.6) and convolving with $g^*(-t)$ yields

$$y_i(t) = e^{j2\pi a_i f_c t} \sum_{n=0}^{N-1} x_i[n] \sum_{p=1}^{P} h_{p,i} e^{-j2\pi f_c \tau_{p,i}} q[(1+a_i)t - nT_s - \tau_{p,i}] + z_i(t) \qquad (4.12)$$

Under no Doppler compensation, $y_i(t)$ is sampled at $t \to mT_s$ at the receiver This yields:

$$y_i[m] = e^{j2\pi a_i f_c m T_s} \sum_{n=0}^{N-1} x_i[n] \sum_{p=1}^{P} h_{p,i} e^{-j2\pi f_c \tau_{p,i}} q[(m-n)T_s - \tau_{p,m,i}] + z_i[m] \qquad (4.13)$$

where $\tau_{p,m,i} = \tau_{p,i} - a_i m T_s$. Using the equivalent channel $f(t,\tau)$ (see section 3.2), this expression is equivalent to

$$y_i[m] = e^{j2\pi a_i f_c m T_s} \sum_{n=0}^{N-1} x_i[n] f[m, m-n] + z_i[m] \qquad (4.14)$$

Substituting (2.4) into (4.14) will result in the expression

$$y_i[m] = \frac{1}{\sqrt{N}} V_i^m \sum_{\ell=0}^{L-1} f[m,\ell] \sum_{k=0}^{N-1} X_i[k] W_N^{-kn} + z_i[m] \qquad (4.15)$$

where $\ell = m - n$, $V_i = e^{j2\pi a_i f_c T_s}$ and $W_N = e^{-j2\pi/N}$.

In vector form this can be written as [7, p. 34]

$$\mathbf{y}_i = \mathbf{V}_i \mathbf{C}_f \mathbf{x}_i = \mathbf{V}_i \mathbf{C}_f \mathbf{F}^{-1} \mathbf{X}_i \qquad (4.16)$$

where $\mathbf{F}^{-1} = \frac{1}{\sqrt{N}} \mathbf{F}^*$ which is the $N \times N$ unitary IDFT matrix with components $\frac{1}{\sqrt{N}} \{W_N^{-kn}\}$, $\mathbf{C}_f$ is the equivalent channel matrix which is circulant due to the CP (defined in (2.10)) with matrix elements $\{f_{m,\ell}\}$, $\mathbf{x}_i = [x_i[0] \cdots x_i[N-1]]^T$, $\mathbf{X}_i =$

$[X_i[0] \cdots X_i[N-1]]^T$, and $\mathbf{V}_i = \text{diag}\left(1, V_i, \cdots, V_i^{N-1}\right)$.

Now the DFT of (4.16) can be calculated:

$$\mathbf{Y}_i = \mathbf{F}\mathbf{V}_i\mathbf{C}_f\mathbf{F}^{-1}\mathbf{X}_i$$
$$= \mathbf{F}\mathbf{V}_i\mathbf{F}^{-1}\mathbf{F}\mathbf{C}_f\mathbf{F}^{-1}\mathbf{X}_i$$

$\mathbf{F}$ is the $N \times N$ unitary DFT matrix with components $\frac{1}{\sqrt{N}}\left\{W_N^{kn}\right\}$. Defining $\mathbf{C}_f^{(f)} = \mathbf{F}\mathbf{C}_f\mathbf{F}^{-1}$, the DFT is therefore given by

$$\mathbf{Y}_i = \mathbf{F}\mathbf{V}_i\mathbf{F}^{-1}\mathbf{C}_f^{(f)}\mathbf{X}_i \tag{4.17}$$

where $\mathbf{Y}_i = [y_0 \cdots y_i[N-1]]$.

The frequency-selective fading component is modelled by the diagonal matrix $\mathbf{C}_f^{(f)}$, while the fast fading, or time-selective component (which is the ICI components due to Doppler shift) is modelled by the matrix $\mathbf{F}\mathbf{V}_i\mathbf{F}^{-1}$, which is actually a circulant matrix. Therefore ICI interferes with the ith received OFDM block in a circulant manner (modulo N). This expression provides a full insight on how UWA channels affect OFDM signals.

4.2   ICI Analysis and Parametrization

There are many ways to analyze inter-carrier interference, or ICI. One way is the following. As was seen in the previous section, the received baseband signal can be represented by many forms. Let $y_i(t)$ be given by (4.11):

$$y_i(t) = \frac{1}{\sqrt{N}}e^{j2\pi a_i f_c t}\sum_{k=0}^{N-1} C(f_k)X[k]e^{j2\pi f_k(1+a_i)t} + \tilde{n}_i(t)$$

where $t \in \left[\frac{iT'+\tau_{p,i}}{1+a_i}, \frac{(i+1)T'+\tau_{p,i}}{1+a_i}\right]$ and, as before, $f_k = k/T = k\Delta f$. As explained in the previous section, the OFDM block duration is scaled by $1/(1+a_i)$, and the Doppler scaling factor is assumed to be constant within the block, but can vary from one block to another.

The Fourier transform at the k'th subcarrier $Y_i(f_{k'})$ of $y_i(t)$ after receive filtering, which corresponds to the demodulator output in the k'th subchannel, is given by

$$Y_i(f_{k'}) = \int_{-\infty}^{\infty} y_i(t)e^{-j2\pi f_{k'}t}dt + Z_i(f) = \int_{\frac{iT'+\tau_{p,i}}{1+a_i}}^{\frac{(i+1)T'+\tau_{p,i}}{1+a_i}} y_i(t)e^{-j2\pi f_{k'}t}dt + Z_i(f_{k'}) \quad (4.18)$$

where $0 \leq k' \leq N - 1$. After rearranging, simplifying and CP removal, $Y_i(f_{k'})$ is found to be

$$Y_i(f_{k'}) = \frac{1}{\sqrt{N}} \frac{1}{1+a_i} C_i\left(\frac{f_{k'}}{1+a_i}\right) \sum_{k=0}^{N-1} X_i[k]\rho_{k',k,i} + Z_i(f_{k'}) \quad (4.19)$$

where

$$\rho_{k',k,i} = e^{j\pi\alpha_{k',k,i}(2i+1)}\mathrm{sinc}(\alpha_{k',k,i}) \quad (4.20)$$

$$\alpha_{k',k,i} = \frac{k - k' + a_i(f_c + f_k)T}{1+a_i} \quad (4.21)$$

A similar expression can be found in [12].

Expression (4.19) is the frequency response of the received signal with interference taken into consideration. Observing this expression, the frequency response can be reinterpreted in the form

$$Y_i(f_{k'}) = \sum_{k=0}^{N-1} Y_{k,i}(f_{k'}) + Z_i(f_{k'}) \quad (4.22)$$

This shows that the received signal is the sum of the interference signals from the different subcarriers and the received signal at the correct subcarrier. Based on this interpretation, $Y_{k,i}(f_{k'})$ is given by

$$Y_{k,i}(f_{k'}) = \frac{1}{\sqrt{N}} \frac{1}{1+a_i} C_i\left(\frac{f_{k'}}{1+a_i}\right) X_i[k]\rho_{k',k,i} \quad (4.23)$$

The ICI components can be separated from the desired subcarrier k' in (4.19):

$$Y_i(f_{k'}) = \frac{1}{\sqrt{N}} \frac{1}{1 + a_i} \left[C_i \left(\frac{f_{k'}}{1 + a_i} \right) X[k'] \rho_{k',k',i} + \sum_{k \neq k'} Y_{k,i}(f_{k'}) \right] + Z_i(f_{k'}) \quad (4.24)$$

For the special case $a_i \ll 1$, $Y_{k,i}(f_{k'})$ simplifies to

$$Y_{i,k}(f_{k'}) \approx \frac{1}{\sqrt{N}} C_i(f_{k'}) X_i[k] \rho_{k',k,i} \quad (4.25)$$

where

$$\alpha_{k',k,i} \approx k - k' + a_i(f_c + f_k)T \quad (4.26)$$

Since $\Delta f / (f_c + f_k) \leq 1$ it follows that the above approximations are also valid when $a_i(f_c + f_k) \ll \Delta f$, in which case $\rho_{k',k',i} \approx 1$.

Based on $a_i(f_c + f_k) \ll \Delta f$ (or $a_i \ll 1$) the expression for $Y_i(f_{k'})$ can therefore be written as

$$\begin{aligned} Y_i(f_{k'}) &\approx \frac{1}{\sqrt{N}} C_i(f_{k'}) X_i[k'] + \frac{T}{\sqrt{N}} \sum_{k \neq k'} Y_{k,i}(f_{k'}) + Z_i(f_{k'}) \\ &\approx \frac{1}{\sqrt{N}} C_i(f_{k'}) X_i[k'] + Z_i'(f_{k'}) \end{aligned} \quad (4.27)$$

where $Z_i'(f_{k'}) = \frac{1}{\sqrt{N}} \sum_{k \neq k'} Y_{k,i}(f_{k'}) + Z_i(f_{k'})$ includes both the noise and the interference components. Since the condition $a_i(f_c + f_k) \ll \Delta f$ also implies that $|\rho_{k',k,i}| \ll |\rho_{k',k',i}|$ (which can be seen from the above expressions for $\rho_{k',k,i}$), the interference term $\sum_{k \neq k'} Y_{k,i}(f_{k'})$ would be very small and thus $Z_i'(f_{k'}) \approx Z_i(f_{k'})$. Therefore the ICI in the channel under the assumption of a small Doppler shift is approximately just additional noise [11].

4.3   Doppler Compensation

After synchronization and Doppler estimation, the receiver performs Doppler compensation. Let the estimated Doppler scaling factor be $\hat{a}$. The main Doppler effect is the one responsible for scaling the OFDM signal duration, which manifests itself in the factor $1 + a_i$. The main Doppler effect can be compensated for via resampling [10, p. 74].

From section 4.1, one important expression for $y_i(t)$ (after receive filtering) is given by

$$y_i(t) = \frac{1}{\sqrt{N}} e^{j2\pi a_i f_c t} \sum_{k=0}^{N-1} C(f_k) X[k] e^{j2\pi f_k (1+a_i)t} + z_i(t)$$

where $t \in \left[\frac{iT' + \tau_{p,i}}{1+a_i}, \frac{(i+1)T' + \tau_{p,i}}{1+a_i} \right]$. After the Doppler scale estimation, the value of $\hat{a}_i$ is used to perform the resampling operation. The resampling operation should result in the conversion $r_i(t) \to r_i \left(\frac{t}{1+\hat{a}_i} \right)$. Let $y_i'(t)$ be the baseband equivalent after resampling. Now, after passband-to-baseband downconversion, $y_i'(t)$ will be given by

$$y_i'(t) = \frac{1}{\sqrt{N}} e^{j2\pi \hat{\epsilon}_i t} \sum_{k=0}^{N-1} C(f_k) X[k] e^{j2\pi f_k \frac{1+a_i}{1+\hat{a}_i} t} + z_i \left(\frac{t}{1+\hat{a}_i} \right) e^{-j2\pi \frac{\hat{a}_i}{1+\hat{a}_i} f_c t} \qquad (4.28)$$

where $\hat{\epsilon}_i = \frac{a_i - \hat{a}_i}{1+\hat{a}_i} f_c$, which is the carrier frequency offset (CFO) due to Doppler shift. A similar expression can be found in [12]. Due to resampling, the domain of $y_i'(t)$ is $t \in \left[\frac{1+\hat{a}_i}{1+a_i} (iT' + \tau_{p,i}), \frac{1+\hat{a}_i}{1+a_i} ((i+1)T' + \tau_{p,i}) \right]$.

The following relationship should be observed in (4.28):

$$y_i'(t) = y_i \left(\frac{t}{1+a_i} \right) e^{-j2\pi \frac{\hat{a}_i}{1+\hat{a}_i} f_c t} \qquad (4.29)$$

It should also be noted that the scaling of the subcarriers has been compensated for at this stage, which reduces (and with enough estimator iterations eliminates) the subcarrier-dependent Doppler shift. Therefore at this stage the narrowband assumption will hold again.

Now the receiver compensates for the residual Doppler shift. The residual Doppler shift is approximately due to the CFO term $e^{j2\pi \hat{\epsilon}_i t}$, and can be compensated for by multiplying $y_i'(t)$ by $e^{-j2\pi \hat{\epsilon}_i t}$ [12, p. 74]. This yields

$$u_i(t) = \frac{1}{\sqrt{N}} \sum_{k=0}^{N-1} C(f_k) X[k] e^{j2\pi f_k \frac{1+a_i}{1+\hat{a}_i} t} + z_i \left(\frac{t}{1+\hat{a}_i} \right) e^{-j2\pi \left(\hat{\epsilon}_i + \frac{\hat{a}_i}{1+\hat{a}_i} f_c \right) t} \qquad (4.30)$$

where $u_i(t) = y_i'(t) e^{-j2\pi \hat{\epsilon}_i t}$, which is the compensated received signal. Now the ICI effects are reduced. With enough iterations of the Doppler scale estimator, the ICI effects will be further minimized, and the received signal will be recovered with no

ICI. The Fourier transform $u_i(t)$ at the k'th subcarrier is given by

$$U_i(f_{k'}) = (1 + \hat{a}_i)Y_i \left[(1 + \hat{a}_i)\left(f_{k'} + \hat{\epsilon}_i + \frac{\hat{a}_i}{1 + \hat{a}_i}f_c\right)\right] \tag{4.31}$$

Doppler compensation can be digitally implemented, which is more practical for OFDM design and implementation. One method is via interpolation and FFT [10, p. 75]. Let $g'(t) = g^*(-t)$, which is the receive filter. By the sampling theorem the expression for $y_i'(t)$ can then be given by

$$y_i'(t) = \sum_{n=0}^{N-1} y[n]e^{-j2\pi\hat{a}_i f_c nT_s} g'\left(\frac{t}{1 + \hat{a}_i} - nT_s\right) \tag{4.32}$$

Sampling at $t \to mT_s$ yields the discrete-time sequence

$$y_i'[m] = \sum_{n=0}^{N-1} y[n]e^{-j2\pi\hat{a}_i f_c nT_s} g'(mT_s' - nT_s) \tag{4.33}$$

where $T_s' = T_s/(1 + \hat{a}_i)$ as expected, which is the resampling operation. Thus at the receiver, the signal needs to be sampled at the sampling rate $f_s' = 1/T_s'$ via sample-rate conversion for the main Doppler scale compensation. Now the residual Doppler shift can be compensated:

$$u_i[m] = y_i'[m]e^{-j2\pi\hat{\epsilon}_i mT_s} \tag{4.34}$$

The received signal is now fully recovered, free of any ICI components. The frequency samples $U_i[k']$ can now be obtained via an N-point FFT.

A more complete representation for $u_i[m]$ that is relevant in this method can be obtained by using (4.12) instead, which includes the matched filter:

$$u_i[m] = \sum_{n=0}^{N-1} x_i[n] \sum_{p=1}^{P} h_{p,i}e^{-j2\pi f_c \tau_{p,i}} q(mT_s' - nT_s - \tau_{p,m,i}) + z_i(mT_s')e^{-j2\pi a_i mT_s'} \tag{4.35}$$

where $\tau_{p,m,i} = \tau_{p,i} - a_i mT_s'$. Synchronization at the receiver should reduce $\tau_{p,m,i}$.

Another digital implementation method for Doppler compensation is via the chirp z-transform (CZT) [10, p. 77]. This method performs the compensation in the frequency domain rather than the two-step approach (main Doppler compensation followed by residual Doppler compensation) taken so far in the time domain. The method works as follows. The Fourier transform of (4.32) is given by

$$U_i(f_k) = T_s(1 + \hat{a}_i) \sum_{n=0}^{N-1} y[n] e^{-j2\pi \hat{a}_i f_c n T_s} e^{-j2\pi(1+\hat{a}_i)\hat{\epsilon}_i n T_s} e^{-j2\pi(1+\hat{a}_i) f_k n T_s}$$

Recalling that $f_k = k/T$, the above expression can be rewritten in the simplified form

$$U_i[k] = \frac{T}{\sqrt{N}}(1 + \hat{a}_i) \sum_{n=0}^{N-1} y_i[n] A_i^n W_N^{(1+\hat{a}_i)kn}$$

where

$$W_N = e^{-j2\pi/N} \tag{4.36}$$

$$A_i = e^{-j2\pi[(1+\hat{a}_i)\hat{\epsilon}_i + \hat{a}_i f_c]T_s} \tag{4.37}$$

where $U_i[k] = \frac{T}{\sqrt{N}} U_i(f_k)$ by digital signal processing properties. Thus the mth received sample has a DFT $U_i[k']$.

The CZT can be evaluated via an N-point FFT. Unlike interpolation and FFT, the CZT method computes the DFT directly from the discrete-time sequence $y[n]$ rather than relying on sample-rate conversion prior to Fourier transformation. This makes the CZT method more efficient and more accurate, since errors can occur in the sample-rate conversion process (especially for large values of a_i) which could distort the received signal.

Chapter 5

OFDM Simulations and Results

This chapter presents simulations of an OFDM system with differential modulation. The simulation models apply the ideas discussed so far, and tests the validity of the various solutions proposed for UWA transmission, namely, OFDM transmission to deal with frequency-selectivity, and the SOS model to randomly generate UWA channels. Doppler compensation is not present in the simulations due to the absence of Doppler estimation in the research; however Doppler estimation will be part of the future work in this research.

The following stages were chronologically followed to arrive at two main models, "OFDMfull" and "OFDM_SOS":

1. A standard uncoded OFDM transmission simulation model was designed first, dubbed "CarrierTest"

2. A turbo coding simulation model was then desgined, dubbed "DQSKTurbo" [7].

3. "CarrierTest" and "DQSKTurbo" were combined to form the coded OFDM simulation model, dubbed "OFDMfull"

4. The SOS simulation model (Figure 3.2), dubbed "SOS," was designed. The code of the SOS model is given in the appendix

5. "SOS" and "OFDMfull" were combined to form the coded OFDM model capable of simulating UWA channels with Doppler effects, dubbed "OFDM_SOS"

The OFDM system model "CarrierTest" is based on the formulation outlined in section 2.1. The "CarrierTest" model is shown in Figure 5.1 below. The transmitter creates a message of symbols to be transmitted and prepares it via modulation, upsampling, filtering and upconversion. The receiver downconverts, filters, downsamples and demodulates the received signal. The figure shows the AWGN block as the

communication channel model through which the signal is sent. To model multipath channels, an FIR filter block is inserted before the AWGN block. The Error Rate Calculation block is used to compare the transmitted message with the received message, and calculates the BER.
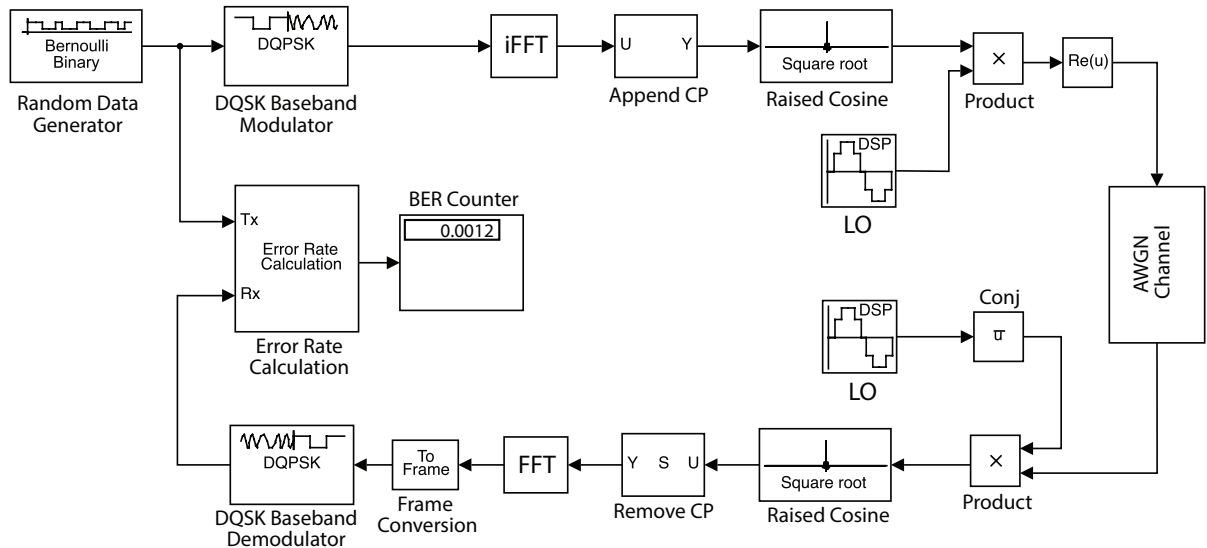

Figure 5.1: "CarrierTest" Simulink model, run with $E_b/N_0 = 9$ dB.

BER curves from simulations are shown in Figure 5.2. The blue curve is the BER from a standard AWGN channel, while the red curve is the BER of a "two-impulse" model that represents a multipath channel. As noted above, an FIR filter models the multipath channel for these simulations.

The multipath channel in the figure has an impulse at the discrete time $n = 0$ carrying 75% of the energy, followed by a second impulse carrying the remaining 25% of the energy at $n = 1$. A low number of carriers was sufficient to simulate this channel, in this case 128. A higher number of carriers would not have improved the performance significantly, since the channel is flat.

Figure 5.2 shows that uncoded OFDM has poor performance. A powerful FEC (Forward Error Correction) code is required, like turbo or LDPC, in order to rectify this and reduce the BER degradation as much as possible. Figure 5.3 shows a rate-1/2 turbo code designed by another member of the research group, and is dubbed
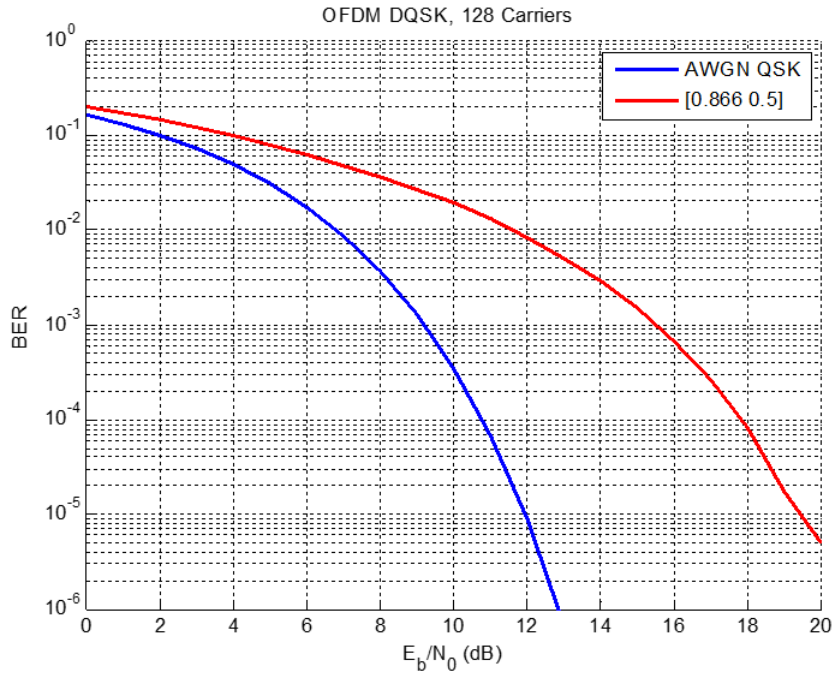
Figure 5.2: "CarrierTest" BER curves for the AWGN channel and three "two-impulse" models.

"DQSKTurbo." This model will be explained in detail to show how it improves "CarrierTest." It is similar in structure to "CarrierTest," but the equivalent channel is modelled semi-analytically by the "Channel Gain" block.

The model uses soft-decision rather than hard-decision demodulation. Soft decision is based on the amplitude of the received symbol in the decision-making process, which takes into account noise effects (bits are anywhere between 0 and 1), unlike hard decision which is only based on the quadrant of the symbol in the constellation diagram (bits are 0's and 1's). Differential demodulation blocks in Simulink can only perform hard decision. On the other hand coherent demodulation blocks can perform hard or soft decisions. Thus the QPSK demodulator block (which uses soft decision) was used with an input of the form $Y[k]Y^*[k-1]$; this is equivalent to a DQPSK demodulator with soft-decision demodulation.

The soft-decision demodulator uses approximate LLRs (Log-Likelihood Ratios). Approximate LLR yields reliable results, while avoiding NaN (Not-a-Number) errors, which appear at high SNRs if exact LLRs are used. This is because exact LLRs involve
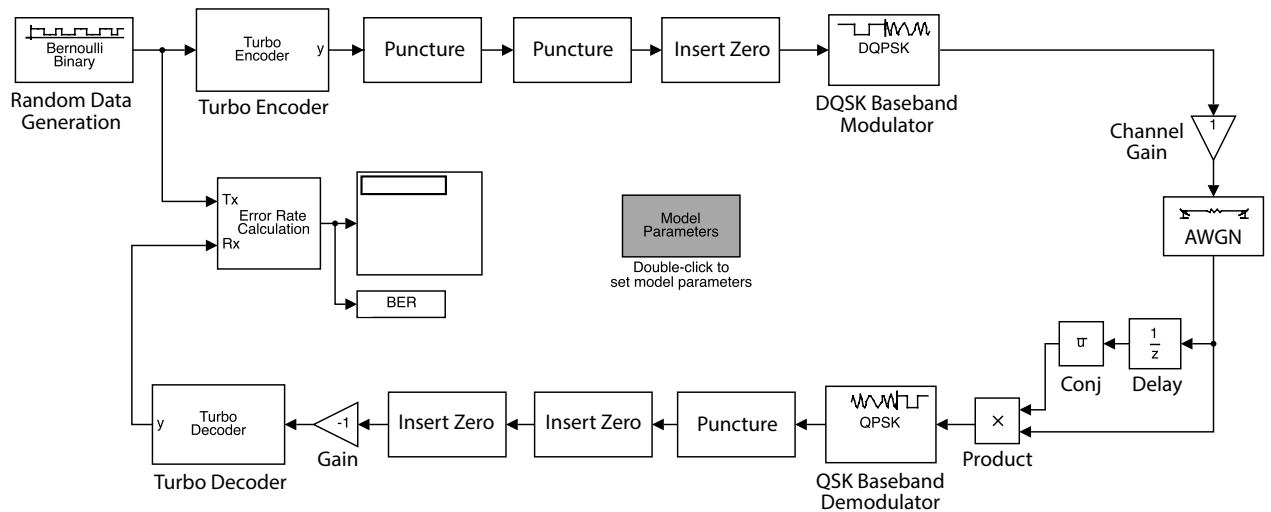
Figure 5.3: "DQSKTurbo" Simulink model, which contains turbo encoding and decoding.

computing exponentials of very large or very small numbers using finite-precision arithmetic, which ultimately results in high BERs [13]. Thus approximate LLRs perform better than exact LLRs at high SNRs since they do not use exponentials; however at low SNRs there is a small difference, which was found to be less than 1%.

The turbo code provided by Simulink is a rate-1/3 code. Also, the turbo interleaving (and deinterleaving) vector provided by Simulink is a linear interleaving (deinterleaving) vector. The coderate was changed to rate-1/2 to improve the effective throughput of the system, and a series of puncture and zero insertion Simulink blocks are used (see Figure 5.3) for this purpose. The linear interleaving vector was changed to a quadrature permutation polynomial (QPP) vector, which provides a higher BER performance due to the higher entropy that the QPP interleaver provides as opposed to a linear interleaver.

The QPP interleaver (and deinterleaver) is an LTE QPP interleaver, and its code is shown below, where `k` is the message length and `p.indices` is the interleaving vector [14]. The scheme is adaptable to any input sequence of length `k=2m` in the range [64:4096]:

```
[f1, f2] = getf1f2(k);
ldx = [0:k-1].';
p.indices = mod(f1*ldx + f2*ldx.^2, k) + 1;
```

After the successful testing of "DQSKTurbo," it was added to "CarrierTest,"
resulting in the coded OFDM simulation model dubbed "OFDMfull." The model is
shown in Figure 5.5. Both "DQSKTurbo" and "OFDMfull" were tested with various
two-impulse channels to confirm that "OFDMfull" gives nearly the same performance
as that of "DQSKTurbo," since "DQSKTurbo" gives the ideal results of turbo coding.

The models were tested under three two-impulse models of the form $h[n, \ell] =
0.866\delta[n] + 0.5\delta[n - \ell]$ where $\ell = 1, 6, 12$. Figure 5.4 shows $h[n, \ell]$ for $\ell = 1$ and
$\ell = 12$. The multipath spread can be made more severe with larger values of ℓ, which
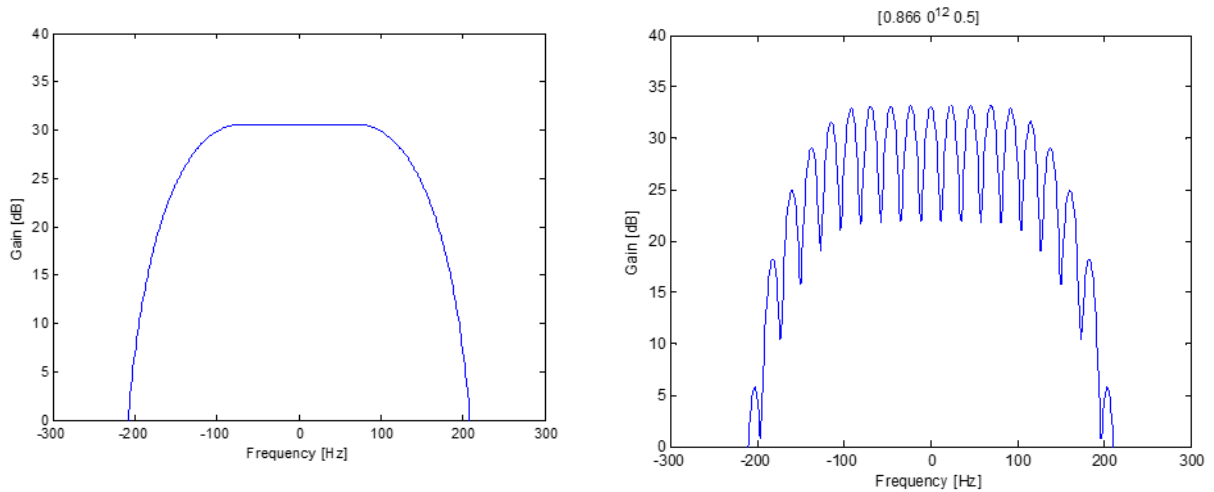effectively worsens the frequency selectivity in the channel.

Figure 5.4: Magnitude response of the channel with a discrete-time multipath spread
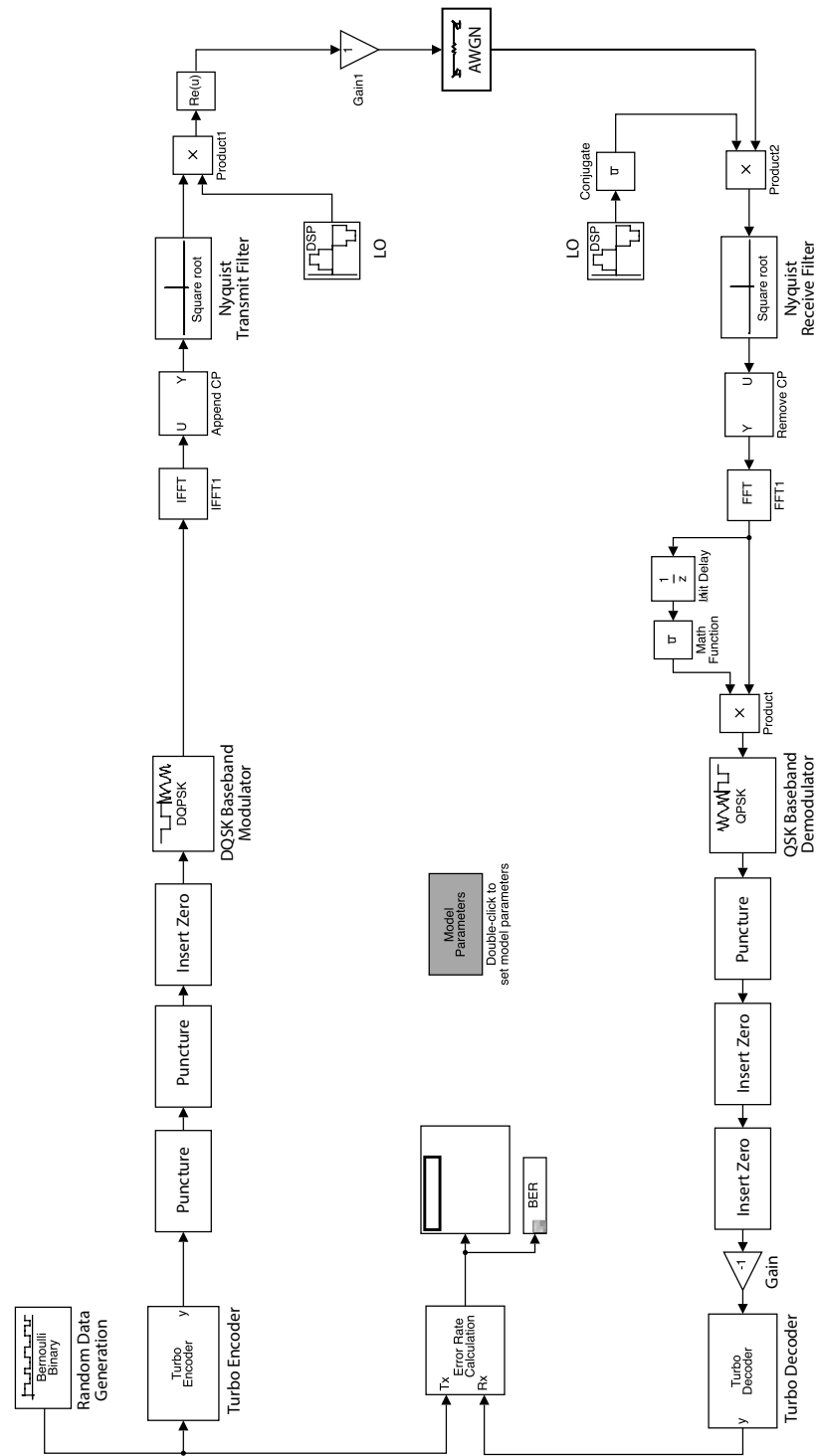of 1 (left) and 12 (right). A higher spread results in more rapid oscillations.

Figure 5.5: The "OFDMfull" model, shown in detail, which includes rate-1/2 turbo coding with soft-decision demodulation added to the "CarrierTest" model.
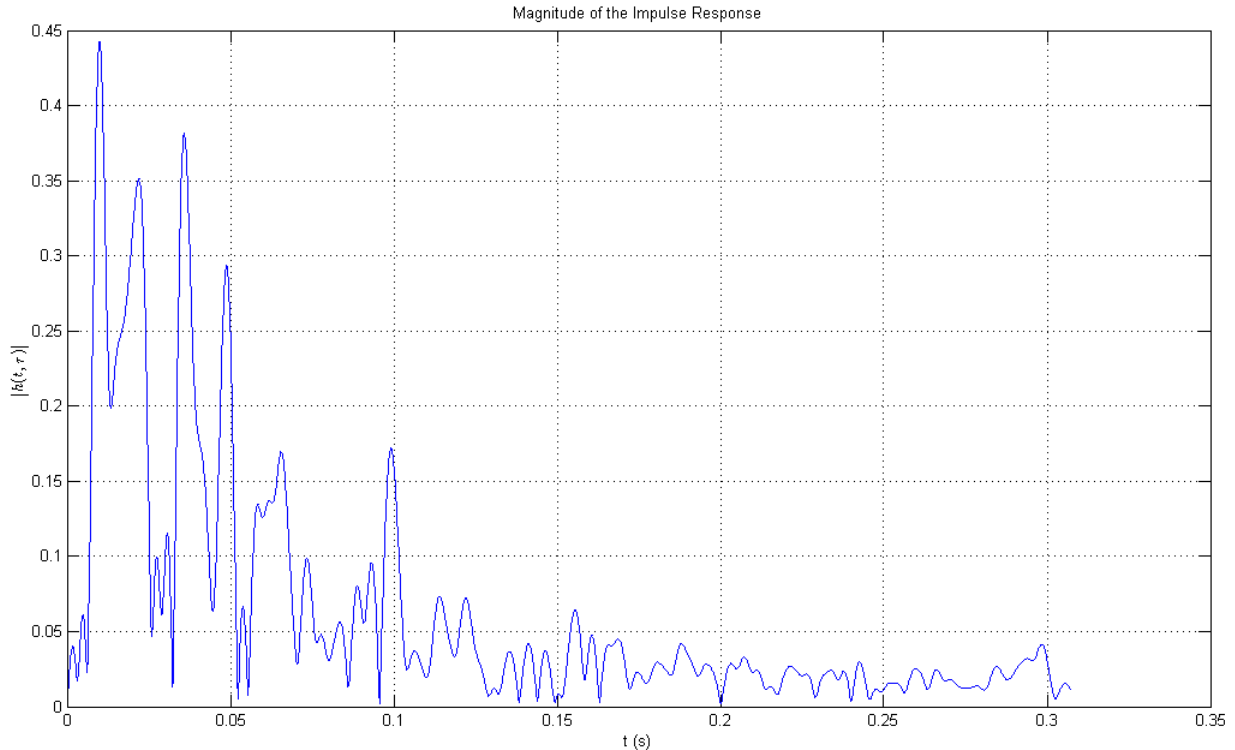
Figure 5.6: Magnitude of the impulse response of the Ultra Electronics' water tank channel. The channel has a multipath spread of about 160 ms.

The model was also tested with Ultra Electronics Maritime Systems Inc.'s tank channel. The magnitdue of the impulse response of the channel is shown in Figure 5.6 and its magnitude response is shown in Figure 5.7. The impulse response shows a multipath spread of about 160 ms (the values between 160 and 300 ms are very small and thus ignored). The channel, just like the received signal, is sampled at 300 Hz. Thus the multipath spread in discrete time is $\ell = 48$. It should be noted that the channel response is quasi-stationary in this setting (i.e. nearly slow fading), presenting primarily frequency-selective fading.

Both models were found to have nearly the same performance. Figure 5.8 shows the BER performance of "DQSKTurbo" and "OFDMfull" under the channels described above. It is observed that the tank channel requires a higher SNR to have low BER as opposed to the other channels. A 10^{-5} BER for the tank channel is achievd for SNR=14 dB, as opposed to the channel shown with the worst spread ($\ell = 12$) which required an SNR of about 11 dB.
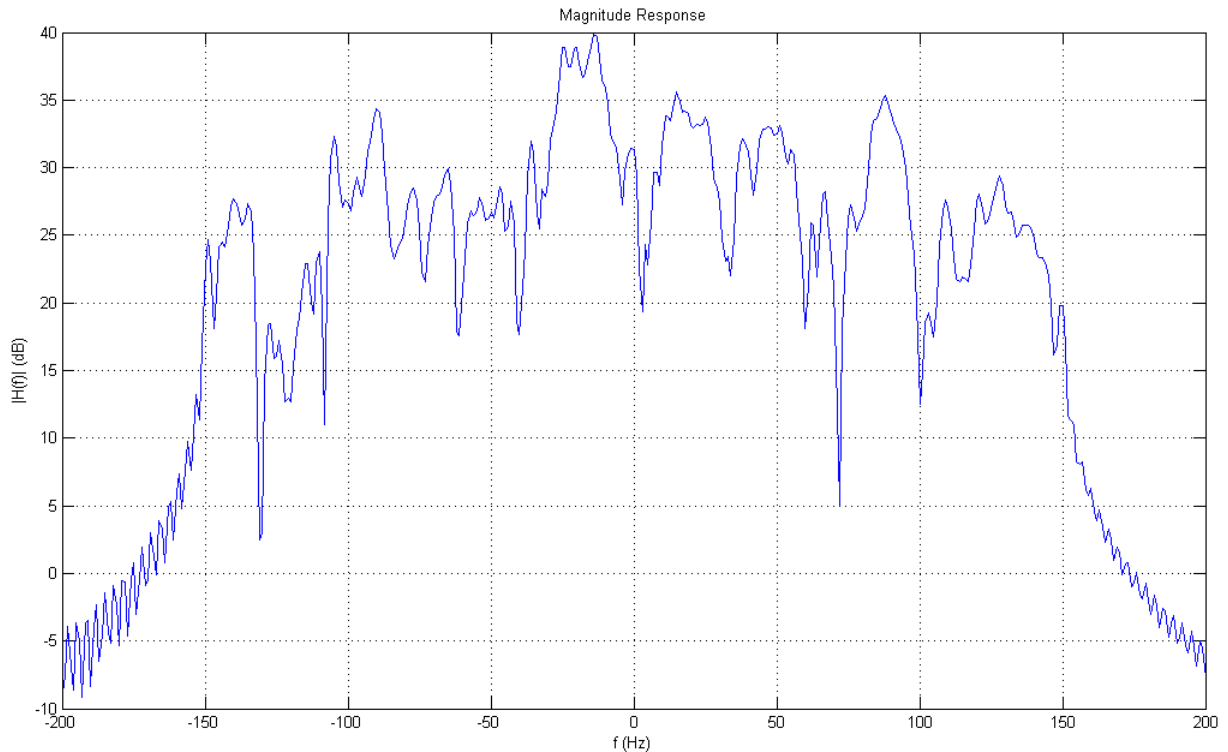
Figure 5.7: Magnitude response of the Ultra Electronics' water tank channel with a signal bandwidth $W = 300$ Hz

Yet, as can be seen from the curves, the error control code effectively avoids the error floor effect. In case of frequency-selective channels, a high number of subcarriers improves performance, which is why 1024 subcarriers were used in the simulations. This is because, for a sufficiently high number of subcarriers, most subchannels will be approximately flat. However, some subchannels would still suffer from fading due to the "holes" present in the channel. Thus at some point, no matter how large the number of subcarriers are, or how large the SNR is, the performance will not change. As a result, this manifests itself as an error floor in the BER performance. These effects are typical for frequency-selective channels, and one of the reasons why error control coding is required for reliable communications.

Finally, the sum-of-sinusoids (SOS) model representation of the channel was added to the simulation environment "OFDMfull" to arrive at another simulation model. The SOS model, explained in section 3.2, is used to model the time-variant UWA channel and its associated Doppler distortion. Thus, the OFDM model with the SOS
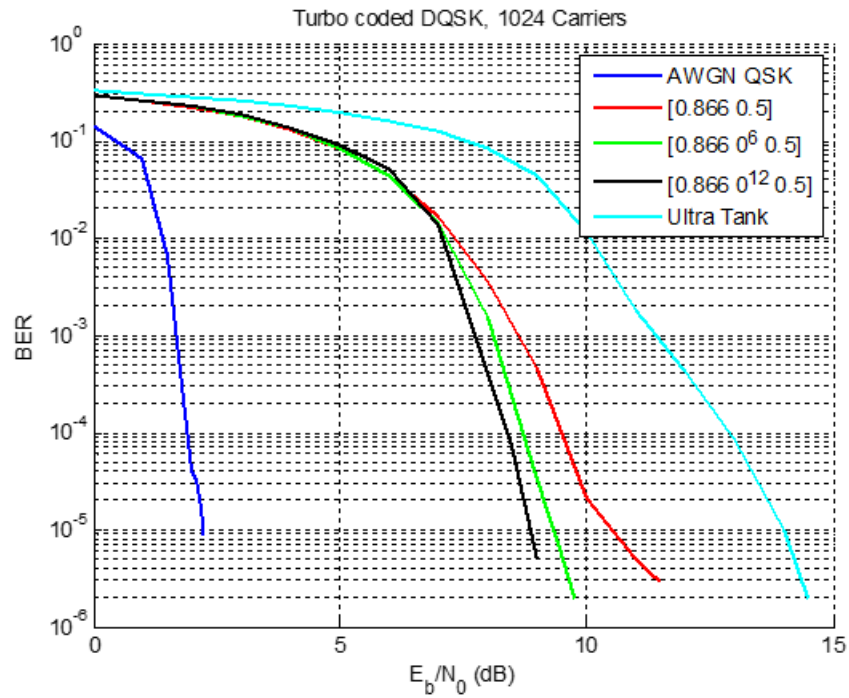
Figure 5.8: "DQSKTurbo" and "OFDMfull" BER curves for the channels described above.

model can be used to obtain results for different multipath channels and doppler spreads. The OFDM model that includes the SOS model for two paths is shown in Figure 5.9, and is dubbed "OFDMSOS." Again, the model yielded the same BER curves as shown above for the corresponding channels.

All the simulations, tests and results obtained in this section were for a static frequency-selective channel setting, where the model (2.11) is applicable. Future work will be directed towards designing Doppler estimators in order to simulate and test the model under Doppler effects. These doppler effects are particularly relevant for the analysis and successful design of OFDM models in UWA channels, as discussed in Chapter 3.
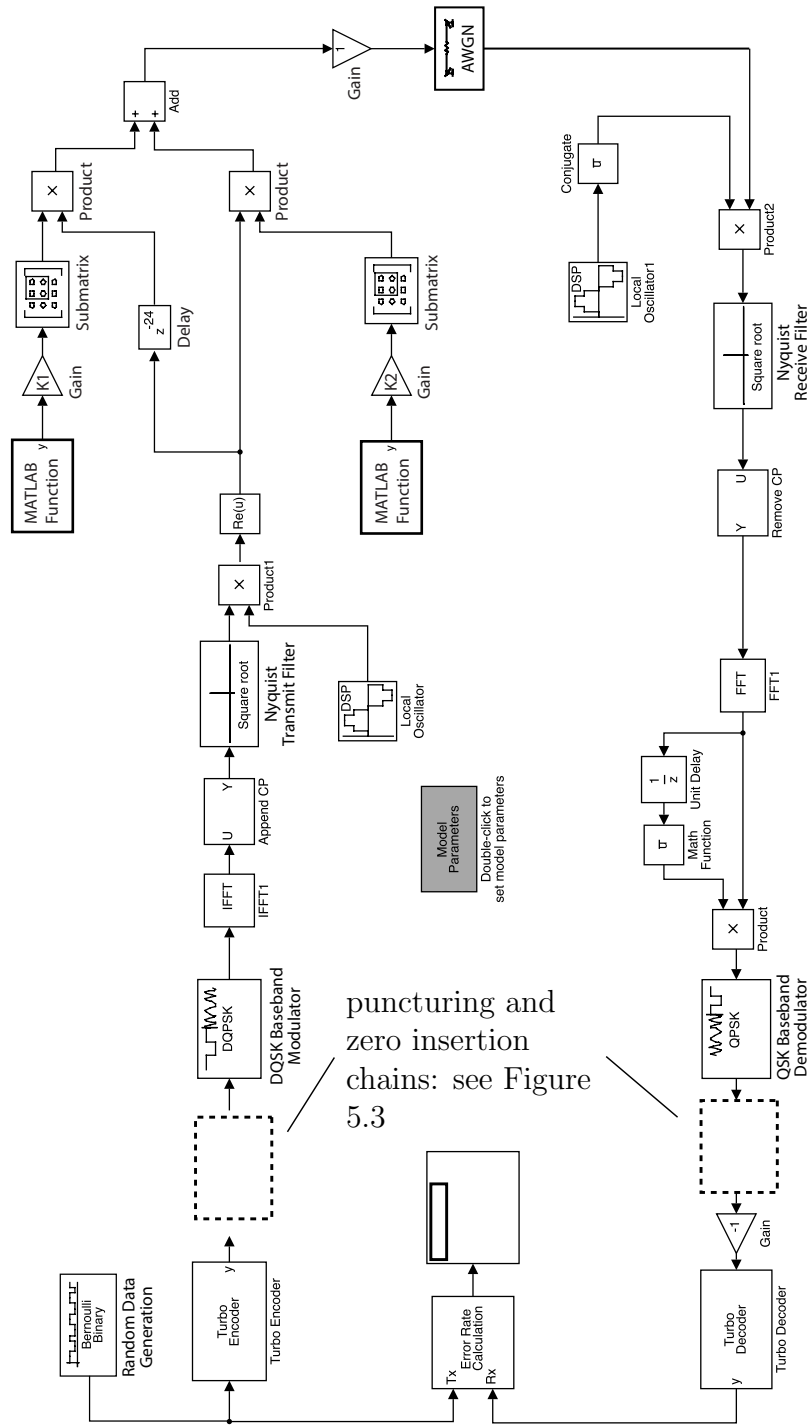
Figure 5.9: The "OFDM_SOS" model, designed by including the SOS channel model in the "OFDMFfull" model.

Chapter 6

Conclusion

The OFDM modulation scheme has been proposed to deal with the frequency selectivity of the UWA channel. The UWA channel has been analyzed and investigated from first principles, and a simplified model of the channel has been proposed, which relies on the narrowband assumption. That is, with the OFDM transmission scheme, the duration of the transmitted OFDM block can be made large enough such that the path's attenuation factor is approximately constant. In other words, the path's impulse response is approximately just an impulse. The narrowband assumption is found to be valid for a large enough number of OFDM subcarriers in the absence of Doppler effects.

The UWA channel has been assumed to be WSSUS, which allows the channel to be characterized with the Doppler spectrum and multipath delay profile, and allows the use of the SOS model to simulate UWA channels under Doppler effects. The Doppler spectrum has been modelled with the stretched exponential function. An SOS simulator has then been proposed that is able to randomly generate time-varying channel taps and Doppler frequencies based on the exponential model, which is a special case of the stretched exponential model.

OFDM transmission on UWA channels was then investigated in detail, with special emphasis on the Doppler effects in the channel. It has been found that the Doppler effects stretch/compress the signal in time; in the frequency domain, it has been found that each subcarrier experiences a different Doppler shift, which also results in shifting/compressing the spectrum. The spectrum has also been found to suffer from Doppler shift in the carrier frequency. Thus the Doppler effect is so severe that the narrowband assumption does not hold anymore if the signal is left with no Doppelr compensation.

A complete and concise model for the received signal has been derived in matrix form which shows the fast fading effects and frequency-selective effects in the channel. The fast fading effects appear as ICI components in the expression, and the frequency-selective effects appear as frequency response components of the equivalent UWA channel. The ICI has also been parametrized, and it has been found that for small Doppler scaling factors, ICI components appear as additional noise in the received signal.

Two digital implementation methods of Doppler compensation have been presented. The first method is via interpolation and FFT. This method relies on resampling the received signal first, and the residual Doppler shift that remains after the resampling process is then compensated for. The second method is via the CZT. The CZT method performs Doppler compensation in the frequency domain and does not rely on resampling. Thus the method is more efficient and accurate, since resampling requires sample-rate conversion at the receiver which may introduce sampling errors that distort the signal. In either case, Doppler compensation eliminates the Doppler effects in the signal, and the narrowband assumption therefore is valid again.

The OFDM simulators designed have been shown to agree with the theoretical results. Since the uncoded OFDM simulator has been found to have poor performance in multipath channels (as expected), the simulator has been upgraded to a coded OFDM simulator via a rate-1/2 turbo coding simulator with soft-decision demodulation. However, due to the absence of a Doppler estimator, Doppler compensation has not been performed at the receiver.

Nonetheless the coded OFDM simulator has been found to have a much better performance under multipath channels, even with a severe multipath spread. The simulator has also been tested with the impulse response of a real UWA channel, and it has again provided a good performance (a BER of 10^{-5} at 14-dB SNR). Finally, another simulator has been desgined by combining the coded OFDM model with the SOS model. This gives a full OFDM simulator capable of modelling OFDM signals on UWA channels with randomly-generated Doppler frequencies.

Bibliography

[1] A. B. Carlson and P. B. Crilly, *Communication Systems: An Introduction to Signals and Noise in Electrical Communication*, New York: The McGraw-Hill Companies, Inc., 2010.

[2] J. G. Proakis and M. Salehi, *Digital Communications*, New York: The McGraw-Hill Companies, Inc., 2008.

[3] H. Schulz and C. Lüders, *Theory and Applications of OFDM and CDMA: Wideband Wireless Communications*, Chichester: John Wiley & Sons, Ltd, 2005.

[4] M. Stojanovic, "Underwater acoustic communications: design considerations on the physical layer," in *Fifth Annual Conference on Wireless on Demand Network Systems and Services*, Jan. 23–25, 2008.

[5] M. Stojanovic, "On the relationship between capacity and distance in an underwater acoustic channel," in *Proc. First ACM International Workshop on Underwater Networks (WuwNet/MobiCom)*, Los Angeles, CA, Sept. 2006.

[6] P. Qarabaqi, "Statistical characterization of a class of underwater acoustic communication channels," Electrical Engineering Dissertations, paper 106, Jan. 2014, Retrieved from `http://hdl.handle.net/2047/d20005071`

[7] Ultra Maritime Digital Communications Centre, *UMDCC Regular Report, December 2014*, 2015, Halifax: Dalhousie University.

[8] P. Hoeher, "A statistical discrete-time model for the WSSUS multipath channel," *IEEE Transactions on Vehicular Technology*, vol. 41, pp. 461-468, Nov. 1992.

[9] P. A. van Walree, T. Jenserud, and R. Otnes, "Stretched-exponential Doppler spectra in underwater acoustic communication channels, *J. Acoust. Soc. Am.*, vol. 128, no. 5, Nov. 2010.

[10] S. Zhou and Z. Wang, *OFDM for Underwater Acoustic Communications*, Chichester: John Wiley & Sons, Ltd, 2014.

[11] "Low complexity OFDM detector for underwater acoustic channels," in *Proc. of MTS/IEEE OCEANS Conference*, Boston, MA, Sept. 18–21, 2006

[12] B. Li, S. Zhou, M. Stojanovic, L. Freitag, and P. Willett, "Multicarrier underwater acoustic communications over fast-varying channels," in IEEE Journal of Oceanic Engineering, vol. 33, No.2, pp.198–209, April 2008.

[13] QPSK Demodulator Baseband, (n.d.), *Demodulate QPSK-modulated data*, Retrieved June 9, 2014, from `http://www.mathworks.com/help/comm/ref/qpskdemodulatorbaseband.html`

[14] H.Zarrinkoub, *Understanding LTE with MATLAB from mathematical modeling to simulation and prototyping*, Chichester: John Wiley & Sons, Ltd, 2014.

Appendix

The 'MATLAB Function' MATLAB Code

```
function y = fcn
% #codegen
% uses Tmax : time from 0 to Tmax
% uses Tdelta : time interval
% uses M : number of micro-paths
% creates v : array of M Doppler frequencies
% generated via INVERSE TRANSFORM SAMPLING
% creates phi : array of M phase offsets
% a is the exponent in the stretched exponential

M=1; Tdelta=1/300; Tmax=1000;
a = 1.207 % Exponential parameter from Ultra measurements,
u=rand(M,1);

% below are the Doppler frequencies for the stretched exponential
% spectrum
if u<=0.5
        v = a*log(2*u);
else
        v = a*log(2-2*u);

phi = rand(M,1);
time = [0:Tdelta:Tmax];
Ns = Tmax/Tdelta+1;
Samples = sum(exp(2*pi*j*(phi*ones(1,Ns)+v*time))/sqrt(size(phi,1)),1);
c_p = Samples';
% Use to plot distribution of Doppler frequencies: hist(v,20)
```